

Engineered 3D Cardiac Fibrotic Tissue to Study Fibrotic Remodeling

*Original*

Engineered 3D Cardiac Fibrotic Tissue to Study Fibrotic Remodeling / Sadeghi, Amir Hossein; Shin, Su Ryon; Deddens, Janine C.; Fratta, Giuseppe; Mandla, Serena; Yazdi, Iman K.; Prakash, Gyan; Antona, Silvia; Demarchi, Danilo; Buijsrogge, Marc P.; Sluijter, Joost P. G.; Hjortnaes, Jesper; Khademhosseini, Ali. - In: ADVANCED HEALTHCARE MATERIALS. - ISSN 2192-2659. - 6:11(2017), pp. 1601434-1601447. [10.1002/adhm.201601434]

*Availability:*

This version is available at: 11583/2703001 since: 2018-03-07T23:03:02Z

*Publisher:*

Wiley-VCH Verlag

*Published*

DOI:10.1002/adhm.201601434

*Terms of use:*

This article is made available under terms and conditions as specified in the corresponding bibliographic description in the repository

*Publisher copyright*

Wiley preprint/submitted version

This is the pre-peer reviewed version of the [above quoted article], which has been published in final form at <http://dx.doi.org/10.1002/adhm.201601434>. This article may be used for non-commercial purposes in accordance with Wiley Terms and Conditions for Use of Self-Archived Versions..

(Article begins on next page)

# 1 **Engineered Three-Dimensional Cardiac Fibrotic Tissue to Study Fibrotic Remodeling**

2 *Amir Hossein Sadeghi*<sup>1,2,3,4†</sup>, *Su Ryon Shin*<sup>1,2,5†</sup>, *Janine C. Deddens*<sup>4</sup>, *Giuseppe Fratta*<sup>1,2,8</sup>, *Serena*  
3 *Mandla*<sup>1,2</sup>, *Iman K. Yazdi*<sup>1,2,5</sup>, *Gyan Prakash*<sup>1,2</sup>, *Silvia Antona*<sup>1,2,8</sup>, *Danilo Demarchi*<sup>8</sup>, *Marc*  
4 *Buijsrogge*<sup>3</sup>, *Joost P.G. Sluijter*<sup>4,6,7</sup>, *Jesper Hjortnaes*<sup>3,6</sup>, *Ali Khademhosseini*<sup>1,2,5,9,10\*</sup>

5  
6 <sup>1</sup>Biomaterials Innovation Research Center, Division of Engineering in Medicine, Department of  
7 Medicine, Brigham and Women's Hospital, Harvard Medical School, Cambridge, MA 02139,  
8 USA.

9  
10 <sup>2</sup>Harvard-MIT Division of Health Sciences and Technology, Massachusetts Institute of  
11 Technology, Cambridge, MA 02139, USA.

12  
13 <sup>3</sup>Department of Cardiothoracic Surgery, Division Heart and Lungs, University Medical Center  
14 Utrecht, Utrecht, Netherlands.

15  
16 <sup>4</sup>Department of Cardiology, Division Heart and Lungs, Laboratory of Experimental Cardiology,  
17 University Medical Center Utrecht, Utrecht, Netherlands.

18  
19 <sup>5</sup>Wyss Institute for Biologically Inspired Engineering, Harvard University, Boston, MA 02115,  
20 USA

21  
22 <sup>6</sup>UMC Utrecht Regenerative Medicine Center, University Medical Center Utrecht, Netherlands.

23  
24 <sup>7</sup>Netherlands Heart Institute (ICIN), Utrecht, Netherlands.

25  
26 <sup>8</sup>Department of Electronics and Telecommunications, Politecnico di Torino, 10129 Torino, Italy.

27  
28 <sup>9</sup>Department of Physics, King Abdulaziz University, Jeddah 21569, Saudi Arabia.

29  
30 <sup>10</sup>Department of Bioindustrial Technologies, College of Animal Bioscience and Technology,  
31 Konkuk University, Hwayang-dong, Kwangjin-gu, Seoul, Republic of Korea.

32  
33 <sup>†</sup>*These authors contributed equally to this work.*

34  
35  
36 Corresponding authors:

37 Biomaterials Innovation Research Center, Division of Engineering in Medicine, Department of  
38 Medicine, Brigham and Women's Hospital, Harvard Medical School, 65 Lansdowne Street,  
39 Cambridge, MA 02139, USA.

40 E-mail address: [alik@bwh.harvard.edu](mailto:alik@bwh.harvard.edu) (Ali Khademhosseini)

41  
42 **Keywords:** Cardiac fibrosis, Cardiac tissue engineering, *In vitro* 3D models, Hydrogels,  
43 Myofibroblast.

44

45 **Abstract**

46 Upon myocardial injury, activated cardiac fibroblasts (myofibroblasts (MyoFs)) play an essential  
47 role in adverse cardiac remodeling, which in the long term cause cardiac fibrosis. As a result,  
48 there is an increased risk of cardiac death due to arrhythmias and heart failure. However, the  
49 abilities to study this process is complicated, as cardiac fibroblasts usually activate  
50 spontaneously into cardiac MyoFs when cultured on two-dimensional (2D) culture plates. Here,  
51 we present a simplified three-dimensional (3D) hydrogel platform of contractile cardiac tissue,  
52 stimulated by transforming growth factor- $\beta$ 1 (TGF- $\beta$ 1), to recapitulate a cardiac fibrogenic  
53 environment. We hypothesized that the quiescent state of cardiac fibroblasts can be controlled by  
54 mimicking the mechanical stiffness of native heart tissue. To test this hypothesis, we created an  
55 *in vitro* 3D cell culture model consisting of primary cardiomyocytes and cardiac fibroblasts  
56 encapsulated within mechanically engineered gelatin methacryloyl (GelMA) hydrogel. We then  
57 characterized the metabolic activity, structure, and contractility of the engineered heart tissue  
58 constructs. Treatment with a beta-adrenergic agonist (isoprenaline) increased beating frequency  
59 in the engineered cardiac tissues, demonstrating physiologic-like behavior of the constructs.  
60 Subsequently, quiescent cardiac fibroblasts within the constructs were activated by the  
61 exogenous addition of TGF- $\beta$ 1. The expression of fibrotic protein markers (collagen I,  
62 fibronectin,  $\alpha$ -smooth muscle actin ( $\alpha$ -SMA)) and the functional changes (eg. proliferation,  
63 arrhythmogenicity) of the fibrotic-like tissues were analyzed to validate the model. This 3D

64 culture model of cardiomyocytes and cardiac fibroblasts exhibited physiological functions of  
65 cardiac tissue and enabled controlled activation of MyoFs, thus demonstrating the usability of  
66 this platform as a 3D culture model to study cardiac fibrotic remodeling. Furthermore, this  
67 platform may be used as a more pathophysiologic-like culture model to study the effects of new  
68 therapeutic agents.

69

## 70 **1. Introduction**

71

72 Cardiovascular diseases (CVDs), such as ischemic heart disease and hypertension, have  
73 remained in the top 10 major causes of death worldwide.<sup>1</sup> Myocardial infarction (MI), which is  
74 responsible for more than 50% of the deaths attributable to CVDs, results in a significant loss of  
75 cardiomyocytes.<sup>2,3</sup> This loss results in the initiation of a reparative wound healing process, which  
76 is characterized by an initial inflammatory phase and followed by the proliferation and activation  
77 of quiescent cardiac fibroblasts into cardiac myofibroblasts (MyoFs).<sup>4</sup> Cardiac fibrosis results  
78 from the excessive synthesis and accumulation of extracellular matrix (ECM) components (eg.  
79 collagen, fibronectin), and is caused by the persistent activation and proliferation of both cardiac  
80 fibroblasts and MyoF (**Fig 1**).<sup>3-9</sup> In addition, cardiac MyoFs (hallmarked by the expression of  $\alpha$ -  
81 smooth muscle actin ( $\alpha$ -SMA)) (**Fig 1**) have contractile properties, which can lead to a sustained  
82 contractile stress that is exerted on the infarcted area.<sup>10,11</sup> In the short term outlook, these pro-  
83 fibrotic processes can be beneficial for cardiac function as it prevents dilatation and rupturing of  
84 the ventricular wall.<sup>12</sup> However, prolonged and excessive activity of MyoFs results in excessive  
85 fibrosis and tissue stiffening, which ultimately impairs cardiac function, increases the risk of  
86 arrhythmia, and leads to the progression of end-stage heart failure.<sup>6,10,13,14</sup>

87           Although there are many identified biochemical (eg. transforming growth factor- $\beta$ 1  
88 (TGF- $\beta$ 1), angiotensin II, endothelin-1, platelet derived growth factor),<sup>4,8,15</sup> mechanobiological,  
89 (eg. tissue stiffness, mechanical strain, and hemodynamic stress)<sup>16,17</sup> and cellular processes (eg.  
90 cardiac fibroblasts migration, MyoF activation)<sup>7</sup> that play a role in cardiac fibrosis, there are a  
91 limited number of therapies available that effectively target fibrosis associated heart disease.<sup>8,10,18</sup>  
92 An important cause of the limited development of improved and more specific therapies against  
93 cardiac fibrosis is the lack of biomimetic *in vitro* platforms to investigate the fibrogenic  
94 remodeling after cardiac injury.<sup>4</sup> A suitable *in vitro* model would preferably maintain cardiac  
95 fibroblasts in a quiescent state and enable the integration of more physiological factors, such as  
96 contractile tissue activity, cell-cell, cell-ECM, and paracrine and hormonal interactions. Thus  
97 there exists a need for a novel, *in vitro* model system to study the pathological changes in  
98 biomimetic and *in vivo*-like conditions. These systems could not only be used for studying  
99 fibrotic changes in heart tissue, but they can potentially contribute to the development of more  
100 physiologically relevant assay systems for drug screening.<sup>19</sup>

101           During the last decade, tissue engineering strategies have shown promise in designing  
102 biomimetic *in vitro* models of cardiac tissue through the use of cardiac cells encapsulated in  
103 three-dimensional (3D) hydrogel-based ECM.<sup>20-22</sup> For instance, the use of a gelatin methacryloyl  
104 (GelMA)-based hydrogel in creating a functional and contractile cardiac tissue was demonstrated  
105 by the successful encapsulation of cardiomyocytes and cardiac fibroblasts in a mechanically  
106 tunable hydrogel.<sup>20,23</sup> Additionally, different natural (eg. collagen, hyaluronic acid) and  
107 synthetic-derived (eg. polyethylene glycol (PEG)) hydrogel culture models have been developed  
108 to control and direct the activation of cardiac fibroblasts and fibroblast-like cells into MyoFs.<sup>24-26</sup>  
109 However, there are still remaining challenges in engineering cardiac-like tissues to study MyoF

110 activation and the associated fibrotic remodeling. To date, most of the model systems that have  
111 been used to study this, were based on either 2D<sup>24</sup> or mono-cultures of cardiac fibroblasts<sup>24,26</sup>.  
112 Similarly, the previously engineered cardiac-like tissues have not been used to study the  
113 pathological remodeling that occurs during cardiac fibrosis. Consequently, some of the crucial  
114 factors that need to be incorporated within *in vitro* culture platforms are different cardiac cells in  
115 an *in vivo* like 3D microenvironment, which can be stimulated (externally) to exhibit a fibrosis  
116 phenotype.

117 In the present study, we developed a 3D hydrogel-platform, composed of cardiomyocytes  
118 and cardiac fibroblasts, which are used to engineer a physiologically relevant *in vitro* platform to  
119 control the activation of cardiac fibroblasts towards MyoF. We hypothesized that by  
120 mechanically tuning the stiffness of the hydrogels, a native-like ECM environment can be  
121 created to enhance the quiescent state of cardiac fibroblasts, and the functional behavior of  
122 engineered cardiac tissues. In addition, the physiological properties of these *in vitro* cardiac  
123 tissues were characterized and the pro-fibrotic consequences of a TGF- $\beta$ 1 induced activation of  
124 cardiac fibroblasts were observed. We believe that this disease model of myocardial fibrosis may  
125 be a suitable *in vitro* model to study bio-mechanistic processes of cardiac fibrosis. Moreover, this  
126 platform could contribute to the development of better biomimetic pre-clinical drug screening  
127 platforms.

## 128 **2. Materials and methods**

### 129 Synthesis of GelMA

130 GelMA was synthesized as described in a previous protocol.<sup>23</sup> Briefly, type A gelatin (10%  
131 (w/v)) from porcine skin (Sigma-Aldrich) was added to Dulbecco's phosphate buffer saline

132 (DPBS; Gibco). This mixture was then stirred and heated at 50 °C for 1h to obtain a clear gelatin  
133 solution. Subsequently, 1.25% (v/v) or 8% (v/v) methacrylic anhydride (Sigma-Aldrich) was  
134 added dropwise to synthesize middle- (MM) and high-degree methacryloyl modification (HM)  
135 GelMA. The solution was stirred and remained on a hot plate for 1h (middle methacryloyl  
136 modification) or 2h (high methacryloyl modification), after which, DPBS was added to stop the  
137 reaction. Following this, the GelMA solution was dialyzed (molecular weight cut off: 12 – 14  
138 kDa) with deionized water for 10 days at 40 °C to remove any salts and unreacted methacrylate  
139 anhydride. Finally, the GelMA solution was filtered (0.2 µm), frozen (-80 °C), and lyophilized  
140 for 5 days to obtain GelMA foam. The foam was stored at room temperature until further  
141 experimental use.

142

#### 143 Preparation of Hydrogel Constructs

144 GelMA pre-polymer solutions were prepared by dissolving 5%, 7%, and 10% (w/v) MM and  
145 HM GelMA in DPBS containing 0.25% (w/v) photoinitiator (PI; Igracure 2595 Sigma). The  
146 solutions were briefly vortexed, and placed in an oven at 80 °C for 15 min to obtain pre-polymer  
147 solutions of GelMA. To prepare disc-shaped hydrogels, 12 µL of the pre-polymer solution was  
148 pipetted between two 600 µm tall spacers and covered with a 3-(trimethoxysilyl) propyl  
149 methacrylate (TMSPMA) treated glass-slide (**Supplemental Fig 1**). This pre-polymer solution  
150 was placed into a customized UV-chamber and exposed to UV light (800 mW, 360-480 nm) for  
151 20 s, resulting in the creation of 600 µm tall hydrogel discs (**Supplemental Fig 1**). After this, the  
152 GelMA hydrogels were removed manually from the glass slide and utilized for further  
153 experiments.

154

### 155 Cardiac Cell Isolation and Culture

156 Primary ventricular cardiomyocytes and cardiac fibroblasts were isolated from two-day-old  
157 neonatal Sprague Dawley rats. These procedures were based on a previously well-defined  
158 protocol approved by the Institution's Committee on Animal Care.<sup>27</sup> Briefly, the hearts of  
159 neonatal pups were surgically removed from the thoracic cavity after euthanasia. Upon removing  
160 the atria, the ventricular tissues were cut into multiple small pieces and incubated overnight (at 4  
161 °C) on a shaker in a 0.05% (w/v) trypsin solution prepared in Hank's Balanced Salt Solution  
162 (HBSS, Gibco, USA). The heart tissues were subjected to four collagenase type II (LS004176,  
163 Worthington, Lakewood, NJ) digestions (10 minutes, 37 °C, 80 rpm) to further digest the heart  
164 tissues. The cell suspension was then collected, centrifuged (1000 rpm) for 5 min, and pre-plated  
165 for 1 h to enrich the cardiomyocytes for immediate experimental use. The attached cardiac  
166 fibroblasts were cultured for a maximum of three passages for future experimental use. The  
167 cardiac fibroblasts were cultured in Dulbecco's Modified Eagle Medium (DMEM, Gibco USA)  
168 with 10% fetal bovine serum (FBS; Gibco, USA) and 1% penicillin/streptomycin (P/S; Gibco,  
169 USA).

170

### 171 Engineering Cell-Laden Hydrogel Constructs

172 To fabricate cell-laden hydrogel constructs, a pre-polymer solution was prepared with minor  
173 modifications to the described protocol above. In brief, 5%, 7%, and 10% (w/v) MM and HM  
174 GelMA was dissolved in DMEM containing 0.25% PI, 50% FBS, 1% P/S, and 2% (w/v) L-  
175 glutamine (Gibco USA). Pre-polymer solutions were removed from the 80 °C oven, and placed

176 in a water bath at 37 °C until cell encapsulation. Cultured cardiac fibroblasts (passage 1-3) were  
177 trypsinized and mixed at a 1:1 ratio with the freshly isolated cardiomyocytes to obtain a final  
178 concentration of  $25 \times 10^6$  cells/mL. The cells were centrifuged at 1200 rpm for 5 min, and the  
179 pellet was resuspended in the GelMA pre-polymer solution. Gels were created following the  
180 preparation of hydrogel constructs (above) and placed in culture medium containing DMEM,  
181 supplemented with 10% FBS, 1% P/S, and 2% L-glutamine. In some conditions, media was  
182 additionally supplemented with TGF- $\beta$ 1 at a concentration of 2 ng/mL (100-21C, PeproTech,  
183 USA) Medium was replaced consistently every 24 h throughout all experimental conditions.

184

#### 185 Characterization of Hydrogels and Engineered Cardiac Tissues

186 Hydrogels were fabricated according to the described methods above to determine the  
187 compressive modulus of the constructed (cell-laden) hydrogels. After fabrication, non-cell-laden  
188 hydrogels were detached from the glass slide and allowed to swell overnight in DPBS at 4 °C.  
189 Engineered cardiac tissues, however, were cultured in normal and TGF- $\beta$ 1 containing medium  
190 for 14 days before mechanical testing (n=5). Hydrogels were cut with a 5 mm biopsy punch, and  
191 excess liquid was removed from the hydrogel. Gels were compressed with a uniaxial tensile  
192 loading machine (Instron, 5542, USA) at a rate of 1mm/min with a 10 N cell load capacity. The  
193 compressive modulus was calculated as the slope from 0-15% strain (n=4).

194 Scanning electron microscopy (SEM; Zeiss Ultra 55 SEM; Carl Zeiss, Thornwood, NY,  
195 USA) was performed to characterize the hydrogel porosity. Cell-laden hydrogels were fixed at  
196 day 1 and day 14 in 4% (v/v) paraformaldehyde (PF, 15700, Electron Microscopy Sciences,  
197 Hatfield, PA) for 30 min at room temperature. Following fixation, the cell-laden hydrogels were  
198 washed with DPBS and incubated at 4 °C overnight. Hydrated hydrogels were placed in liquid

199 nitrogen for 20 min and stored at -80 °C overnight. After freezing, the hydrogels were  
200 lyophilized for 2 days to obtain a porous and foam-like GelMA hydrogel. The foams were  
201 broken in half and coated with Pt/Pd to allow for cross-sectional imaging by SEM.  
202 Quantification of the pore-size was performed by measuring pore-size diameter (n=150) from  
203 SEM images (n=3) made from 5% HM, 7% MM, and 10% MM GelMA foams.

204 Hydrogel degradation was assessed by fabricating hydrogels and subjecting them to collagenase-  
205 induced degradation. Hydrogels were fabricated and allowed to swell in DPBS overnight at 4 °C.  
206 Hydrogels were then placed in a 0.5 U/mL collagenase type II solution (in DPBS) at 37 °C.  
207 Excess liquid was removed, and the hydrogels were weighed before and after incubation with  
208 collagenase. The weight loss percent was determined after 0.5, 1, 3 and 6 h (n=3).

209

#### 210 Characterization of Cell Spreading and Cell Viability

211 Cell spreading within the 3D engineered cardiac tissues was determined by visualizing the  
212 organization of F-actin fibers within the cells. The cell-laden hydrogels were fixed with 4% PF  
213 solution for 30 min. Subsequently, the 3D encapsulated cells were permeabilized with 0.1% X-  
214 100 Triton (Sigma-Aldrich) for 40 min at room temperature. This was followed by 45 min  
215 incubation with Alexa Fluor 488 Phalloidin (Invitrogen) with a 1:40 dilution in DPBS. Cell  
216 nuclei were counterstained with 4',6-diamidino-2-phenyl indole dihydrochloride (DAPI; Vector  
217 Laboratories) for 20 min at room temperature. Hydrogels were then washed three times in DPBS  
218 for 5 min. 3D imaging was performed by confocal microscopy (Leica SP5 X MP, Germany) to  
219 visualize the fluorescently stained F-actin fibers and to determine the degree of cell spreading  
220 within the hydrogels. Z-stack (100 µm each) images were taken of each hydrogel per condition

221 and four areas (400  $\mu\text{m}$  x 400  $\mu\text{m}$ ) were selected for further quantification of cell spreading.  
222 Fractional area coverage by F-actin was determined within the four selected windows using  
223 ImageJ software.

224 Cell viability was examined with a Live/Dead fluorescent labeling kit (Invitrogen) on day 1  
225 of culture according to the manufacturer's protocol. Hydrogels were first washed with DPBS  
226 followed by an incubation with calcein-AM (0.5  $\mu\text{L}/\text{mL}$ ) and ethidium homodimer-1 (2  $\mu\text{L}/\text{mL}$ )  
227 in DPBS for 15 min at 37  $^{\circ}\text{C}$ . After washing with DPBS, fluorescent images were taken from 4  
228 selected areas using an inverted microscope (Nikon TE 2000-U, Nikon instruments Inc., USA).  
229 To quantify viability, images were taken at 4 different focal planes within the hydrogel by  
230 adjusting the height of the objective manually. Three cell-laden hydrogels were used to  
231 determine the cell viability in each condition, and ImageJ software was used to quantify the  
232 number of viable cells. Data depicted represents the percentage of live cells within the  
233 engineered constructs. Cell metabolic activity was assessed throughout culture with PrestoBlue<sup>®</sup>  
234 Cell Viability Reagent (PB; Life Technologies). The cell-laden hydrogels were incubated with  
235 PrestoBlue for 2 h at 37  $^{\circ}\text{C}$  in a 1:10 dilution in normal culture medium (n=4). The fluorescence  
236 was determined (560 nm – 590 nm) using a fluorescence reader (Synergy HT-Reader, BioTek,  
237 Winooski, VT). The data was normalized to hydrogel samples without encapsulated cells. The  
238 data represent the normalized fluorescence absorbance at day 1, 5, 10, and 14 of culture.

239

#### 240 Cell Proliferation Analysis

241 Click-iT Plus EdU Alexa Fluor<sup>®</sup> 488 Imaging Kit (Life Technologies) was used to specifically  
242 and quantifiably assess the number of proliferating cells within 3D cardiac tissues. Proliferating  
243 cells were labeled following the manufacturer's guidelines. Briefly, cell-encapsulated hydrogels

244 (n=3) were incubated with  $10 \times 10^{-6}$  M EdU in normal culture medium at 37 °C. After 24 h of  
245 incubation, the samples were fixed with 4% PF (30 min) and permeabilized with 0.1% X-100  
246 Triton (40 min) at room temperature. The samples were blocked with 3% (w/v) bovine serum  
247 albumin (BSA; Sigma-Aldrich) solution and subsequently incubated for 30 min with the Click-iT  
248 solution at room temperature. Additionally, cell-specific proliferation was assessed by  
249 immunostaining with vimentin, a mesenchymal cell specific marker. Subsequently, the samples  
250 were washed twice with DPBS and counterstained for 20 min with DAPI at room temperature.  
251 3D z-stack (50  $\mu$ m each) images were taken by confocal microscopy. To quantify proliferation,  
252 fluorescence images were taken with an inverted microscope at 3 different focal planes within  
253 the hydrogel by adjusting the height of the objective manually (n=3). ImageJ software was used  
254 to count the number of EdU positive cells. Positive control for EdU labeling was determined by  
255 staining cardiac fibroblasts cultured for 24 h in normal, and TGF- $\beta$ 1 supplemented culture  
256 medium (n=3). Fluorescence images were taken from each sample by using an inverted  
257 microscope (n=10). The percentage of proliferating cells was calculated by counting the EdU  
258 labeled cells using ImageJ software. Cell proliferation was calculated by dividing the EdU  
259 positive cells by the total number of DAPI positive cells.

260

### 261 Immunofluorescence Staining for Cardiac (fibrosis) Specific Markers

262 The 3D engineered cardiac tissues were immunostained for cardiac tissue (sarcomeric  $\alpha$ -actinin,  
263 connexin-43) and cardiac fibrosis ( $\alpha$ -SMA, collagen type I, fibronectin, and matrix-  
264 metalloproteinase-2 (MMP-2)) markers. Samples were fixed with a 4% PF solution for 30 min,  
265 followed by three washing steps (5 min each) with DPBS. Subsequently, the cell-hydrogels were

266 permeabilized by incubation with 0.1% X-100 triton for 45 min, after which the samples were  
267 washed with DPBS and blocked for 30 min with a 10% goat serum solution in DPBS. After  
268 blocking, the hydrogels were incubated with a monoclonal mouse anti-sarcomeric  $\alpha$ -actinin  
269 (Abcam, catalogue #9465), polyclonal rabbit anti-connexin-43 (Abcam, catalogue #11370),  
270 monoclonal rabbit anti-vimentin (Abcam, catalogue #92547), monoclonal rabbit anti- $\alpha$ -SMA  
271 (Abcam, catalogue #32575), polyclonal rabbit anti-collagen I (Abcam, catalogue #292),  
272 polyclonal rabbit anti-fibronectin (Abcam, catalogue #23751), or a polyclonal rabbit anti-  
273 MMP-2 (Abcam, catalogue #37150) for 16 h at 4 °C. After incubation with the primary antibody  
274 (diluted 1:200 in 10% goat serum), the samples were washed three times (10 min each) in DPBS  
275 at room temperature. The secondary antibodies (goat anti-rabbit Alexa Fluor 594 or goat anti-  
276 mouse Alexa Fluor 488 (Abcam)) were diluted 1:200 in 10% goat serum, followed by incubation  
277 with the samples for 2 h at room temperature. The nuclei were counterstained with DAPI.  
278 Immunofluorescence double staining was performed by incubating two primary antibodies (eg.  
279 sarcomeric  $\alpha$ -actinin and connexin-43) simultaneously. After washing with DPBS three times,  
280 the secondary antibodies were incubated separately for 2 h each. 3D confocal z-stack images  
281 (150  $\mu$ m each) were taken and processed with ImageJ software.

282

### 283 Characterization of the Beating Behavior of Engineered Cardiac Tissue

284 The beating behavior of 3D engineered cardiac tissues was characterized quantitatively by using  
285 a temperature controlled chamber (at 37 °C) and real time video recording with a camera (Sony  
286 XCD-X710) attached to an inverted optical microscope. Videos of the beating constructs (n=3)  
287 were recorded every day from day 3 of culture onwards. The beating pattern and frequency of

288 the constructs was determined by a custom written MATLAB program.<sup>28</sup> The single cell beating  
289 characteristics of the engineered tissues, cultured in growth medium supplemented with TGF- $\beta$ 1,  
290 were also assessed with a modified custom written MATLAB program.

291

### 292 GelMA Hydrogel Contraction Assay

293 A GelMA hydrogel contraction assay was performed to assess the contractile manifestation of  
294 MyoFs inside the engineered fibrotic-like cardiac tissues. The GelMA hydrogel contraction assay  
295 was performed in a similar manner as a previously described collagen contraction assay.<sup>24</sup>  
296 Briefly, 3D cell-laden hydrogels were fabricated as described above and were cultured in TGF-  
297  $\beta$ 1 containing culture medium for 14 days according to the protocol. After 14 days, the culture  
298 medium was aspirated and optical images were taken, followed by a quantitative analysis of the  
299 gel diameters using ImageJ software. Depicted data represents mean  $\pm$  SD of gel diameter in  
300 each condition (n=5).

301

### 302 Real-Time Polymerase Chain Reaction for Expression of Cardiac Fibrosis Markers

303 Cell-laden hydrogels were used to examine the expression of cardiac fibrosis markers. First, 3D  
304 cardiac tissues were mechanically disrupted and total RNA was extracted from all samples using  
305 TRIzol reagent (Life Technologies) and total RNA yield was measured with a NanoDrop  
306 (Thermo Scientific). 1  $\mu$ g of total RNA from each sample was reverse transcribed according to  
307 the manufacturer's instructions using the QuantiTect  $\text{\textcircled{R}}$  Reverse Transcription kit (Qiagen). All  
308 RT-PCR was performed using the iTaq<sup>TM</sup> Universal SYBR $\text{\textcircled{R}}$  Green supermix (Bio-Rad, USA).  
309 The 20  $\mu$ L volume reaction component included 10  $\mu$ L supermix, 1  $\mu$ L of primer mix (5  $\mu$ M

310 forward/reverse primer), 100 ng template and nuclease free water (variable). Predesigned  
311 KiCqStart<sup>®</sup> SYBR<sup>®</sup> Green primers (Sigma-aldrich) were obtained for the following target genes:  
312 Collagen1A1 (catalogue #KSPQ12012G), Fibronectin (catalogue #KSPQ12012G),  $\alpha$ -SMA  
313 (catalogue #KSPQ12012G), and MMP-2 (catalogue #KSPQ12012G). Relative expressions were  
314 calculated using  $\Delta\Delta C_t$  method and normalized to glyceraldehyde-3-phosphate dehydrogenase  
315 (GAPDH) gene expression.

316

### 317 Statistical Analysis

318 The quantitative results on all sample conditions were plotted by mean  $\pm$  standard deviation  
319 (error bars). To perform statistical analysis, a student's t-test or one-way ANOVA was used. For  
320 multiple comparisons, we used a Tukey's test. Graphpad Prism (v.6, GraphPad, USA) software  
321 was used to perform all statistical analyses and results were considered to be significantly  
322 different with a  $p < 0.05$ .

## 323 **3. Results**

### 324 3.1 Engineering and Characterization of GelMA Scaffolds

325 The elastic moduli of a healthy neonatal rat heart ranges from 4 to  $\sim 11$  kPa.<sup>29</sup> In this study, we  
326 encapsulated cells from neonatal rat hearts in a GelMA-based hydrogel to engineer 3D  
327 myocardial tissues *in vitro*. The hydrogels showed an increased stiffness with increasing  
328 methacryloyl modification degree and macromer concentration (**Fig 2A**). As such, 10% HM-  
329 GelMA hydrogel exhibited the highest mechanical stiffness ( $25.76 \pm 6.07$  kPa) compared to all  
330 other hydrogel conditions ( $p < 0.05$ ). However, 7% HM-GelMA hydrogel ( $12.97 \pm 2.12$  kPa)

331 showed a significantly higher compressive modulus than 7% MM-GelMA hydrogel ( $4.48 \pm 0.76$   
332 kPa) ( $p < 0.05$ ) and a significantly lower compressive modulus when compared to 10% HM-  
333 GelMA hydrogel. This verifies that the mechanical stiffness can be tuned by varying the  
334 methacryloyl modification degree and macromer concentration of GelMA independently.<sup>23</sup> The  
335 following three hydrogels 5% HM-GelMA ( $9.76 \pm 4.48$  kPa), 7% MM-GelMA ( $4.48 \pm 0.76$   
336 kPa), and 10% MM-GelMA ( $7.25 \pm 1.38$  kPa), exhibited a mechanical stiffness that was in the  
337 range of native neonatal rat hearts (**Fig 2A**) and were therefore further characterized.

338 To access the effect of the GelMA macromer concentration and methacryloyl modification  
339 degree on the morphology of hydrogel, all SEM samples were prepared by same cryogenic  
340 treatment. SEM images indicated that all three selected hydrogels showed highly microporous  
341 structure (**Fig 2**).<sup>30</sup> There is a significant decrease in porosity with an increased macromer  
342 concentration. In addition, a significantly lower porosity was observed in the 5% HM-GelMA  
343 hydrogel as compared to the 7% and 10% MM-GelMA hydrogels (**Fig 2B**). This indicates an  
344 inverse relationship between porosity and degree of methacryloyl modification and macromer  
345 concentration. Although there was a significant decrease in the porosity of 5% HM-GelMA  
346 hydrogel, no significant increase was observed in the mechanical properties of 5% HM-GelMA  
347 hydrogel when compared to 7% and 10% MM-GelMA hydrogels (**Fig 2A**).

348 In native cardiac tissue, MMPs are excreted and activated by cells to induce and promote the  
349 cleavage of ECM components.<sup>31</sup> These proteins play an important role in the maintenance and  
350 remodeling of the heart ECM. To assess the presence of physiological binding substrates for an  
351 MMP-mediated degradation of the GelMA-based scaffold, a degradation assay was performed  
352 with collagenase type II (also known as MMP-8). The results revealed significantly faster  
353 degradation – described as percentage of weight loss – of 5% HM-GelMA hydrogel after 3 and 6

354 h when compared to 10% MM-GelMA hydrogel ( $p < 0.05$ ). Furthermore, a complete degradation  
355 of all three hydrogels was observed after 15 h of incubation with MMP-8 (**Fig 2C**). These results  
356 confirm the existence of MMP substrates in the GelMA hydrogel but also indicate the  
357 opportunity for use of GelMA based scaffolds for engineered physiological heart ECM tissue.

358

### 359 3.2 GelMA Hydrogel Characteristics Affect Cell Spreading but not Viability

360 To determine what hydrogel condition enabled the best cellular spreading and networking, we  
361 investigated the spreading of encapsulated cells inside the three selected GelMA hydrogels. To  
362 visualize this, fluorescent confocal z-stack images were taken after F-actin (cytoskeletal fiber)  
363 staining of the cell-laden hydrogels (**Fig 3A**). After 10 days of culture, the fluorescence images  
364 demonstrated that the majority of the cells inside 5% HM-GelMA and 10% MM-GelMA  
365 hydrogels had limited spreading, as the cells retained a round shape. Interestingly, the expression  
366 of F-actin fibers throughout the 7% MM-GelMA hydrogel clearly demonstrated an increase in  
367 cellular spreading and networking (**Fig 3A**). A higher cellular spreading was expected due to a  
368 lower methacryloyl modification degree and macromer concentration, thereby allowing for an  
369 increased degradation and spreading throughout the ECM by the cells. Therefore, a higher  
370 cellular spreading and networking in 7% MM-GelMA hydrogel could be attributed to the lower  
371 macromer concentration and degree of methacryloyl modification as compared to 10% MM-  
372 GelMA and 5% HM-GelMA hydrogels, respectively. Additionally, a quantitative analysis of the  
373 area covered by F-actin fibers confirmed a significantly higher percentage of fractional coverage  
374 in 7% MM-GelMA hydrogel ( $74.98 \pm 17.70$  %) compared to 5% HM-GelMA ( $22.71 \pm 4.66$  %)  
375 and 10% MM-GelMA ( $42.68 \pm 8.98$  %) hydrogels at day 10 of culture ( $p < 0.05$ ) (**Fig 3B**).

376 The viability of encapsulated cells in the different conditions was also assessed after one day of  
377 culture. This time point was chosen to evaluate the survival of cells following UV exposure  
378 during the fabrication of the constructs. **Figure 3C** depicts the quantitative analysis of the  
379 percentage of live cells at day 1 of culture. Across all experimental conditions, the percentage of  
380 live cells was higher than 84% and was not significantly different between groups.

381

### 382 3.3 Functional Properties of the 3D Engineered Cardiac Tissues

383 For further experiments, we selected the 7% MM-GelMA hydrogel for having the best spreading  
384 and networking features for the cells. Additionally, we studied the viability of cells in this  
385 condition for 2 weeks of culture. The results revealed that the engineered cardiac tissues  
386 remained viable throughout a culture period of 14 days (**Fig 4A**). Compared to day 1, there was a  
387 significant increase in the metabolic activity after 14 days (**Fig 4A**) ( $p < 0.05$ ). Given the fact  
388 that cardiomyocytes have limited proliferative capacity<sup>20</sup>, we believe that cardiac fibroblasts  
389 were responsible for the increase in metabolic activity.

390 On day 14, we also assessed the phenotype of the encapsulated cardiomyocytes and cardiac  
391 fibroblasts by immunostaining with sarcomeric  $\alpha$ -actinin and vimentin. As depicted in **Figure**  
392 **4B**, a confocal z-stack image of an immunostained cell-laden GelMA hydrogel displayed both  
393 sarcomeric  $\alpha$ -actinin and vimentin positive cells. In addition, we investigated the expression of  
394 connexin-43, a gap junction protein that is important for electrical coupling of cardiomyocytes  
395 and is typically found in the cardiac tissue.<sup>32</sup> From the confocal image in **Figure 4C**, it is clear  
396 that cardiomyocytes demonstrated the expression of both connexin-43 and sarcomeric  $\alpha$ -actinin.  
397 The expression of gap-junctions and functional electro-mechanical coupling was also confirmed

398 by the observation of spontaneous, synchronous, and cardiac tissue-like contraction of the  
399 engineered 3D cardiac tissues (**Supplemental Video 1**). Spontaneous individual cell beating  
400 activity began after 2 days of culture; however, videos of the beating were recorded and analyzed  
401 from when synchronous and tissue-like contraction began (**Fig 4D**). The engineered cardiac  
402 tissues maintained synchronous and tissue-like contraction for as long as 18 days of culture  
403 (**Supplemental Video 2**). Additionally, quantitative analysis of synchronous beats per minute  
404 (BPM) revealed that the constructs reached a maximum of 48 ( $\pm 19.75$ ) BPM on day 10  
405 (**Supplemental Video 3**) and a minimum of 13 ( $\pm 5.57$ ) BPM on day 18 of culture. This variable  
406 beating behavior is consistent with previously reported studies on engineered GelMA-based  
407 cardiac tissues *in vitro*.<sup>20,33,34</sup> The decrease in beating rate with increasing culture time was also  
408 shown in previous studies, in which rat neonatal cardiomyocytes were cultured on hydrogel-  
409 based tissue-engineered models.<sup>27,35</sup> In one of these studies, it was hypothesized that this  
410 decrease might be attributable to the phenotypical transition of fetal cardiomyocytes towards the  
411 neonatal stage.<sup>27</sup> We further went on to analyze the beating pattern of the beating constructs. As  
412 depicted in **Figure 4E**, the cardiac tissues showed a stable and regular beating pattern throughout  
413 culture days 4, 8, 12, and 16.

414 To assess physiological functionality of the engineered cardiac tissues, we also investigated the  
415 effect of a beta-adrenergic drug, isoproterenol (isoprenaline), on the beating behavior on day 6.  
416 Videos of the beating samples were recorded before and after 45 min incubation with 1  $\mu$ M  
417 isoproterenol. An analysis of the videos revealed that the cardiac tissues exhibited physiological  
418 behavior in response to the drugs (**Supplemental Video 4 and 5**). **Figure 4F** and **4G** show the  
419 synchronous beating pattern (and amplitude) and beating frequency (in beats/min), respectively,  
420 of the cardiac tissues before and after the administration of the drug. In the presence of

421 isoproterenol, the cardiac tissues developed a significant increase in their spontaneous beating  
422 frequency (**Fig 4F**). Furthermore, an increase in the amplitude of all the samples was observed  
423 after exposure to the drug (**Fig 4G**).

424

### 425 3.4 TGF- $\beta$ 1 Induces Proliferation of Cardiac Fibroblasts

426 TGF- $\beta$ 1 is a well characterized protein in the pathophysiology of cardiac fibrosis, and is a potent  
427 stimulator of cardiac fibroblast proliferation during the course of this disease.<sup>15</sup> In order to assess  
428 the effect of TGF- $\beta$ 1 on cell proliferation within our engineered 3D cardiac tissues, we analyzed  
429 cell proliferation by EdU labeling. Fluorescent z-stack images of the EdU labeled cardiac tissues  
430 were taken on day 1, 7, and 14 of culture (**Fig 5A**). To identify the cellular phenotype of  
431 proliferating cells, we stained the cardiac fibroblasts by positive immunostaining for vimentin  
432 (**Fig 5A**). From **Figure 5A**, it is clear that the EdU labeled cells (green) were also positively  
433 stained by vimentin (red), thus confirming that the increase in proliferation across the two culture  
434 conditions was attributed to the proliferation of cardiac fibroblasts. Furthermore, a quantitative  
435 analysis of the percentage of EdU stained cells, revealed that the TGF- $\beta$ 1 treated samples  
436 showed a significantly higher number of EdU positive cells compared to the non-treated samples  
437 on day 1 and 7 (**Fig 5B**) ( $P < 0.05$ ). However, there was no significant difference on day 14  
438 between the percentage of EdU positive cells in TGF- $\beta$ 1 treated ( $41.63 \pm 11.31$  %) and non-  
439 treated samples ( $42.45 \pm 10.11$  %). Additionally, the percentage of EdU labeled cells in the non-  
440 treated samples had a significant increase by day 14 ( $42.45 \pm 10.11$  %) compared to day 1  
441 ( $16.74 \pm 3.70$  %) (**Fig 5B**) ( $p < 0.05$ ). A positive control analysis of the proliferation was also  
442 obtained by the EdU labeling of TGF- $\beta$ 1 treated and non-treated cardiac fibroblasts after 24h of

443 2D-seeding in a well-plate (**Supplemental Fig 2**). As expected, the results were consistent with  
444 the results from the engineered cardiac tissues.

445

### 446 3.6 Characterization of the Expression of Cardiac Fibrosis Markers

447 Quiescent cardiac fibroblasts spontaneously differentiate into activated MyoFs when cultured in  
448 conventional 2D tissue culture polystyrene (TCPS) plates (**Supplemental Fig 3A**).  
449 Consequently, no significant difference was found in the expression of fibrotic markers after  
450 incubation of these cells with TGF- $\beta$ 1 for 24h (**Supplemental Fig 3A, B**). This is thought to be  
451 partly due to the higher mechanical stiffness (GPa range) of TCPS compared to native and even  
452 fibrotic myocardium.<sup>16,36</sup> To investigate the activation of cardiac fibroblasts in a 3D beating  
453 heart-like environment and stiffness, we analyzed the expression of a specific MyoF protein  
454 marker,  $\alpha$ -SMA after 14 days of culture (**Fig 6A**). As depicted in **Figure 6A**, cells in the cell-  
455 laden hydrogels showed a minimal expression of  $\alpha$ -SMA, indicating that cardiac fibroblasts  
456 within the cardiac tissues remained in a quiescent state when cultured in normal culture medium.  
457 However, engineered 3D cardiac tissues cultured in the presence of TGF- $\beta$ 1, exhibited a more  
458 MyoFs-like phenotype after 14 days, as can be seen in **Figure 6A**. Furthermore, we analyzed the  
459 expression of other cardiac fibrosis markers by positive immunofluorescence staining of  
460 collagen-I, fibronectin, and MMP-2. Overall, confocal z-stack images clearly demonstrated an  
461 increased expression of fibronectin and collagen-I inside the engineered 3D cardiac tissues  
462 cultured in TGF- $\beta$ 1 supplemented medium. However, the expression MMP-2 was not clearly  
463 increased in the TGF- $\beta$ 1 treated samples. In addition to qualitative protein expression analysis,  
464 we also investigated the mRNA expression of  $\alpha$ -SMA, collagen-I, fibronectin, and MMP-2 by

465 quantitative real time polymerase chain reaction (RT-PCR) to confirm the upregulation of  
466 fibrotic protein expression in the TGF- $\beta$ 1 stimulated samples (**Fig 6B**). The expression levels of  
467  $\alpha$ -SMA, collagen-I, and fibronectin were shown to be elevated for TGF- $\beta$ 1 stimulated samples  
468 when compared to normal growth medium. The greatest increase was observed in the fibronectin  
469 samples, where the mRNA expression was  $3.84 (\pm 2.33)$  ( $p < 0.05$ ) times higher in the TGF- $\beta$ 1  
470 treated samples as compared to the control group. Additionally, mRNA expression levels of  $\alpha$ -  
471 SMA and collagen-I were shown to be  $2.51 (\pm 1.21)$  ( $p < 0.05$ ) and  $3.48 (\pm 1.55)$  ( $p < 0.05$ )  
472 times higher, respectively, in TGF- $\beta$ 1 cultured samples as compared to control medium.  
473 However, as demonstrated by the protein expression analysis (**Fig 6A**), the expression of MMP-2  
474 was not significantly changed in TGF- $\beta$ 1 stimulated samples ( $1.01 \pm 0.53$ ). Altogether, these  
475 results indicated that a quiescent cardiac fibroblast phenotype could be effectively cultured in a  
476 mechanically tuned GelMA-based cardiac tissue construct. Moreover, these results demonstrated  
477 that the phenotypic state of cardiac fibroblasts can be directed by designing a 3D cardiac tissue  
478 with a physiological co-culture of cells and an *in vivo*-like dynamic contraction.

479

### 480 3.5 Analysis of the TGF- $\beta$ 1 induced Pro-Fibrotic Changes

481 During fibrotic remodeling there is a higher risk of arrhythmogenicity as a result of an increased  
482 ECM deposition and an altered electrical-coupling between cardiomyocytes and MyoFs.<sup>13,37</sup> In  
483 addition, human fibrotic cardiac tissue is hallmarked by an increased mechanical stiffness (~30-  
484 70 kPa) when compared to healthy myocardial tissue (~10 kPa).<sup>38,39</sup> Furthermore, MyoFs can  
485 generate a higher contractile force than cardiac fibroblasts and thereby induce contraction and  
486 scarring of the cardiac tissue. We hypothesized that the engineered cardiac tissues would exhibit

487 some of these fibrotic characteristics when the fibrotic response is simulated. To assess the pro-  
488 fibrotic changes, we cultured the samples in normal culture medium and added TGF- $\beta$ 1 for 14  
489 days. All TGF- $\beta$ 1 stimulated cardiac tissues showed spontaneous individual cell beating, from  
490 day 7 to day 13. Video analysis of the beating behavior revealed that there was a non-  
491 synchronous and irregular contraction of all the tissues when stimulated with TGF- $\beta$ 1 (**Fig 7A**  
492 and **Supplemental Video 6**). These results correlated well with previous reports that MyoFs  
493 induce changes in the beating behavior of cardiomyocytes.<sup>13,37</sup>

494 Compared with normal culture medium, we also observed a significant decrease of ~17 % in the  
495 average diameter of the GelMA-based cardiac tissues, thus indicating an increase in the MyoF-  
496 mediated contraction of the hydrogel (**Fig 7 B, C**) ( $p < 0.05$ ). In addition, SEM images of both  
497 culture conditions showed that cardiac tissues from TGF- $\beta$ 1 stimulated samples clearly had a  
498 more fibrous and fibrillar structure than cardiac tissues in the control group (**Fig 7D**). This is  
499 thought to be mainly attributable to the elevated deposition of ECM components (eg. collagen-I,  
500 fibronectin) in the fibrotic-like tissues. On day 14, the mechanical stiffness of TGF- $\beta$ 1 treated  
501 engineered 3D cardiac tissues was compared to cardiac tissues cultured in normal culture  
502 medium. These measurements revealed an increase in the mechanical stiffness of TGF- $\beta$ 1  
503 stimulated encapsulated cells in GelMA hydrogels (**Fig 7E**).

504 Our findings highlight the opportunity to use these GelMA-based engineered 3D cardiac tissue  
505 constructs to identify fibrotic changes, and to study the pathophysiological cells and factors that  
506 play a role in cardiac remodeling and myocardial fibrosis.

507

508 **Discussion**

509 For many decades, conventional TCPS plates have successfully contributed to a better  
510 understanding of fibrogenesis in the context of cardiovascular diseases. However, these models  
511 lack the *in vivo* like presence of tissue-level properties (such as cell-ECM interactions).  
512 Furthermore, cardiac fibroblasts cultured in a 2D TCPS plate, spontaneously activate into MyoFs,  
513 thereby complicating the ability to study phenotypical changes of these cells during disease  
514 development. In this work, we designed a simplified 3D *in vitro* model of cardiac fibrosis by  
515 tuning the mechanical ECM of engineered cardiac tissues followed by stimulating these  
516 hydrogel-based tissues with TGF- $\beta$ 1; an established and potent mediator in fibrotic remodeling.<sup>15</sup>  
517 During cardiac fibrosis, there is an increased synthesis and deposition of ECM components,  
518 including collagen (mainly type I and III), laminin, fibronectin, and elastin.<sup>4,40</sup> During this  
519 process, the main effector cells are activated MyoFs and proliferating cardiac fibroblasts. In  
520 addition, there is an increased (early phase remodeling) and decreased (late phase remodeling)  
521 production and activation of MMPs, which play a role in the degradation of the ECM.<sup>31,41</sup> This is  
522 of importance since it can enable and facilitate the migration of cells (eg. cardiac fibroblasts) to  
523 the area of injury at the early phases of wound healing.<sup>42</sup> The elevated expression of pro-fibrotic  
524 genes such as collagen-I, fibronectin, and  $\alpha$ -SMA in our stimulated cardiac tissue was consistent  
525 with the pathological changes that occur during cardiac fibrosis. Similarly, we observed an  
526 activation of quiescent cardiac fibroblasts by positively immunostaining  $\alpha$ -SMA; a widely used  
527 marker of MyoFs.<sup>43</sup> Immunostaining images further revealed that the TGF- $\beta$ 1 stimulated tissues  
528 also increased the expression of collagen-I and fibronectin. Our results also indicated that there  
529 was an induced proliferation of cells in the TGF- $\beta$ 1 treated cardiac tissues, as identified by EdU  
530 labeling. It is well established that TGF- $\beta$ 1 is an inducer of cardiac fibroblast activation during  
531 pathological fibrotic remodeling.<sup>44</sup> In addition, TGF- $\beta$ 1 is a proliferative stimulator of cardiac

532 fibroblasts.<sup>44,45</sup> Therefore, we investigated whether the proliferating cells are cardiac fibroblasts  
533 or cardiomyocytes by simultaneously labeling with EdU and immunostaining specifically for  
534 cardiac fibroblasts. Our results showed that the proliferating cells were cardiac fibroblasts rather  
535 than cardiomyocytes, which have a low proliferative capacity.<sup>46</sup>

536 This disease model also showed that it could recapitulate functional properties of MyoFs and  
537 fibrotic cardiac tissue. TGF- $\beta$ 1 induced stimulation of the functional cardiac tissues resulted in  
538 an asynchronous and irregular beating behavior. Furthermore, the increased conversion of  
539 cardiac fibroblasts into MyoFs, resulted in a higher contraction and shrinkage of the 3D GelMA  
540 hydrogels. This however, could also be a result of degradation of GelMA hydrogel due to the  
541 production of various MMPs in the TGF- $\beta$ 1 stimulated tissues.

542 GelMA hydrogels have been a widely used scaffolding biomaterial in the past few years for  
543 applications ranging from tissue engineering<sup>33</sup>, organs-on-a-chip,<sup>47</sup> and *in vitro* disease models.<sup>25</sup>  
544 Most of these studies take advantage of the easy fabrication methods, high and easy accessibility,  
545 and high biocompatibility of GelMA hydrogels.<sup>23</sup> Moreover, GelMA hydrogels can be tuned  
546 mechanically to obtain a physiologically relevant stiffness.<sup>23,48</sup> This can be obtained by varying  
547 the macromer concentration, the degree of methacryloyl modification, the concentration of  
548 photoinitiator, the UV intensity, or the UV exposure time.<sup>23</sup> Although GelMA hydrogel is a  
549 semi-synthetic, photocrosslinkable scaffolding material, it provides relevant biomimetic cues of  
550 the native ECM, such as RGD-binding peptides and MMP degradable sites.<sup>49</sup> In addition, gelatin  
551 is a denatured form of collagen, which is the main constituent of native heart tissue, and  
552 therefore exhibits comparable biocompatible and biomimetic properties to collagen. However, a  
553 limitation of this *in vitro* system is the lack of other ECM components that are present in the  
554 native heart (eg. collagens, glycosaminoglycans, laminin, and elastin). Interestingly, previous

555 studies have shown that it is possible to engineer functional cardiac tissue by using naturally  
556 derived decellularized ECM from native heart tissues.<sup>50,51</sup> In a recent study, Visser *et al.* have  
557 combined the fabrication methods of GelMA molecules to engineer crosslinkable hydrogels  
558 derived from various native tissues.<sup>52</sup> Thus indicating that in future work, it could be possible to  
559 combine the advantages of GelMA hydrogels with the native properties of a decellularized heart  
560 ECM.

561  
562 Mechanotransduction is a process in which cells sense their mechanical microenvironment and  
563 transmit the physical stresses of their surroundings to biochemical signals that result in various  
564 cellular outputs (eg. differentiation, proliferation).<sup>53-55</sup> These mechano-physical signals are  
565 mainly mediated through cell-ECM and cell-cell connections, which are converted to cellular  
566 signaling pathways by integrins, focal adhesions, and cadherins.<sup>4,53,56</sup> Cardiac fibroblasts and  
567 cardiomyocytes can sense their extracellular microenvironment by attaching to their ECM with  
568 focal adhesions.<sup>57</sup> Increasing ECM stiffness or ECM-induced strain, can affect both  
569 cardiomyocytes and cardiac fibroblasts in a way that alters contractile function and stimulates  
570 MyoFs activation.<sup>16,58</sup> Consequently, the mechanical stiffness of the extracellular  
571 microenvironment of cardiac tissue is an important factor in both normal physiology and cardiac  
572 fibrosis. In fact, in a previous study by Engler *et al.* it was reported that cardiomyocytes cultured  
573 on stiff, fibrotic-like (34 kPa) substrates, showed a decreased beating activity and lacked the  
574 development of well-striated sarcomere structures.<sup>39</sup> In addition, results from other recent studies  
575 have demonstrated that the mechanical stiffness of the matrix or substrate can facilitate the  
576 transition of cardiac fibroblasts into MyoFs.<sup>24,26</sup> Zhao and colleagues engineered PEG-substrates  
577 with varying degrees of stiffness to study the migration, proliferation, and activation of quiescent

578 cardiac fibroblasts in a 2D *in vitro* model system.<sup>24</sup> This culture platform suggested that the  
579 quiescent state of cardiac fibroblasts could be maintained and directed by mechanically tuning a  
580 hydrogel-based substrate. These results highlight the importance of the tunability of matrix  
581 stiffness for the engineering of functional and contractile cardiac tissues, while simultaneously  
582 maintaining the quiescent-like phenotype of cardiac fibroblasts. In this study, we used 7% MM-  
583 GelMA hydrogel ( $4.48 \pm 0.76$  kPa) to engineer a physiological stiffness in the same range of  
584 native neonatal rat hearts (4-11 kPa).<sup>29</sup> We showed that neonatal rat cardiac fibroblasts remained  
585 in a quiescent-state while co-cultured with cardiomyocytes in a mechanically tunable 3D  
586 hydrogel model.

587 Cardiac muscle is a syncytium in which a network of cardiomyocytes and cardiac fibroblasts are  
588 connected to each other electrically and mechanically. In order to engineer a physiologic-like  
589 heart tissue *in vitro*, it is essential for cardiomyocytes and cardiac fibroblasts to interact with  
590 each other through both direct, and indirect cell-cell and cell-ECM interactions. Here, we  
591 hypothesized that the spreading and networking of cells over time would lead to the development  
592 of a system which better mimics native cardiac tissue. Consequently, 7% MM-GelMA hydrogel  
593 was selected as a 3D substrate for culturing cardiac fibroblasts and cardiomyocytes. The  
594 expression of cardiac differentiation markers (sarcomeric  $\alpha$ -actinin, connexin-43) demonstrated  
595 a well-developed electrical coupling and contractile apparatus inside these hydrogel conditions.  
596 Although the cardiomyocytes had an isotropic orientation inside GelMA hydrogel, there was a  
597 clear elongation and a well-defined sarcomeric structure visible. In native cardiac tissue however,  
598 the cardiomyocytes are elongated and aligned in anisotropic layers of muscle tissue.<sup>59</sup> This is  
599 important for the anisotropic propagation of electrical signals, which plays a critical role in  
600 synchronous and rhythmic cardiac contraction.<sup>60,61</sup> One limitation of our engineered cardiac

601 tissue was the lack of cellular anisotropic alignment, which could potentially lead to impaired  
602 electrical pulse propagation and contraction in comparison to the native heart muscle. In future  
603 studies, we could overcome this through the use of engineering strategies by applying  
604 topographical and electrical cues to the tissues to enhance the elongation and alignment of  
605 cells.<sup>62,63</sup>

606 In this work, we used neonatal rat cardiomyocytes and cardiac fibroblasts to model an *in vitro*  
607 platform of myocardial fibrosis. Currently, the use of rats for *in vitro* studies of heart disease is  
608 the standard in both academia and the pharmaceutical and biotechnology industry. Therefore,  
609 this indicates that our model may be a suitable and pre-clinically relevant *in vitro* platform for  
610 studies of pathophysiology and drug screening applications. However, we recognize the  
611 simplicity of this *in vitro* platform, as it lacks the incorporation of other dynamic (eg. blood flow)  
612 and physiological factors (eg. blood vessels, inflammatory cells), which are present in the native  
613 heart. Recently, microfluidic organs-on-a-chip have emerged and demonstrated the possibility of  
614 incorporating several dynamic factors (such as fluid flow and mechanical stretch) within  
615 microengineered cardiac tissues.<sup>64,65</sup> Further development of microfluidic techniques and tissue  
616 engineering strategies could therefore aid in the creation of a more physiologically relevant  
617 cardiac tissue in the future.

## 618 **Conclusion**

619 In this study, we engineered a simplified but functional and physiologic-like heart tissue to study  
620 cardiac fibrosis in a 3D GelMA-based hydrogel platform. By tuning the mechanical stiffness of  
621 GelMA hydrogels, we were able to create a well-defined and beating network of cardiomyocytes  
622 and quiescent cardiac fibroblasts. Subsequently, we showed that we were able to stimulate the

623 activation of cardiac fibroblasts into MyoFs by adding TGF- $\beta$ 1 to the culture medium.  
624 Furthermore, our results demonstrated that the engineered fibrotic tissues presented electrical and  
625 mechanical alterations that are comparable to fibrotic heart tissues. In conclusion, our study  
626 presents a physiologic-like *in vitro* model of cardiac fibrosis that could enhance our  
627 understanding of this disease, while increasing the potential of these systems to be used for pre-  
628 clinical drug screenings.

629

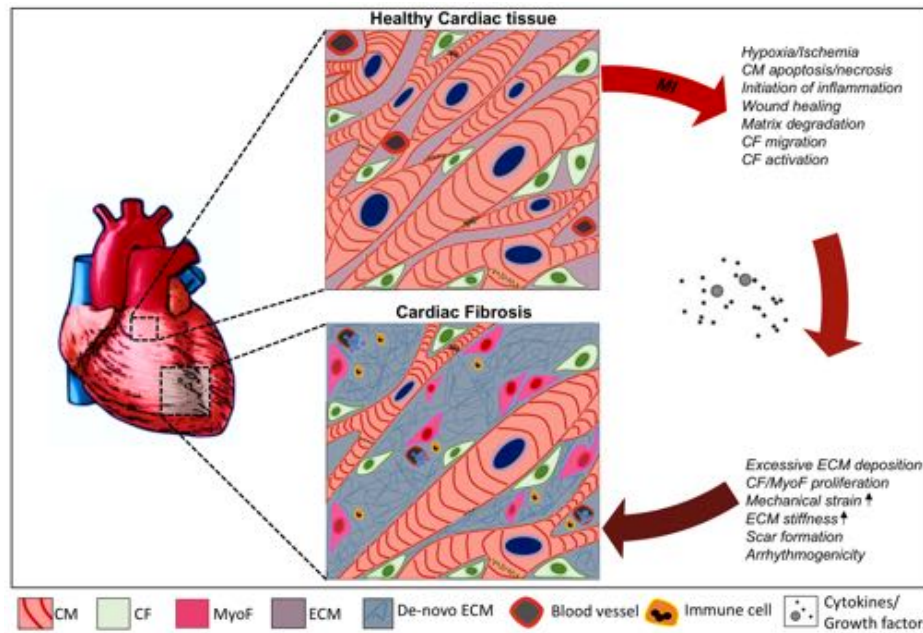
### 630 **Acknowledgements**

631 The authors declare no conflict of interests in this work. The authors gratefully acknowledge  
632 funding by the Defense Threat Reduction Agency (DTRA) under Space and Naval Warfare  
633 Systems Center Pacific (SSC PACIFIC) Contract No. N66001-13-C-2027. The authors also  
634 acknowledge funding from the Office of Naval Research Young National Investigator Award,  
635 the National Institutes of Health (EB012597, AR057837, DE021468, HL099073,  
636 R56AI105024), and the Presidential Early Career Award for Scientists and Engineers  
637 (PECASE). We acknowledge the support from Innovation and the Netherlands CardioVascular  
638 Research Initiative (CVON): The Dutch Heart Foundation, Dutch Federation of University  
639 Medical Centers, the Netherlands Organization for Health Research and Development and the  
640 Royal Netherlands Academy of Science. The publication of this material does not constitute  
641 approval by the government of the findings or conclusions herein. S.R.S. would like to recognize  
642 and thank Brigham and Women's Hospital President Betsy Nabel, MD, and the Reny family, for  
643 the Stepping Strong Innovator Award through their generous funding. I.K.Y. was support by a  
644 NIH Organ Design and Engineering Training fellowship (T32 EB16652).

645

646

CONFIDENTIAL



648

649 **Figure 1. Schematic illustration of the pathophysiological changes during fibrotic cardiac**

650 **remodeling.** Healthy myocardial tissue consists of a network of cardiomyocytes (CM) and

651 quiescent cardiac fibroblasts (CF) that are interspersed within the extracellular matrix (ECM).

652 After myocardial injury (eg. myocardial infarct (MI)), CMs die and a reparative inflammatory

653 and wound healing process is initiated by the release of various cytokines and growth factors

654 (such as transforming growth factor- $\beta$ 1, angiotensin-II etc.). This results in the activation of

655 cardiac fibroblasts into cardiac myofibroblasts (MyoF). These cells and other resident cardiac

656 fibroblasts are responsible for an excessive and prolonged synthesis and deposition of de-novo

657 ECM proteins (eg. collagen-I, fibronectin, laminin). This results in scarring of the heart tissue

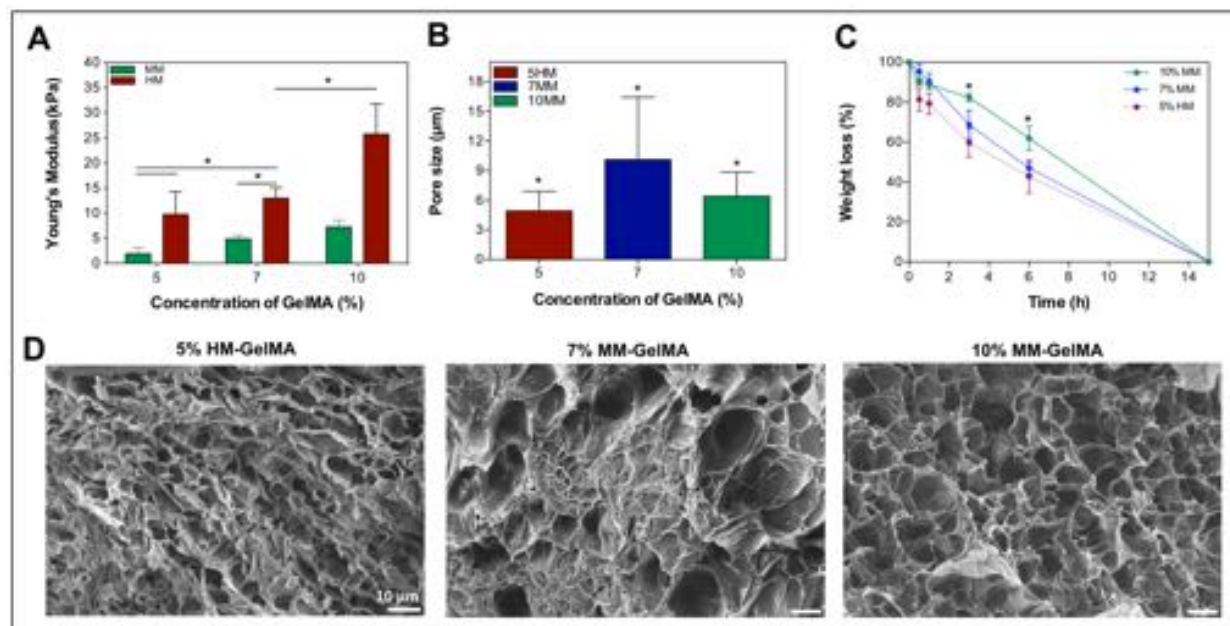
658 and leads to the deterioration of ventricular function followed by diastolic and systolic

659 ventricular dysfunction and may eventually lead to life threatening arrhythmogenicity or heart

660 failure.

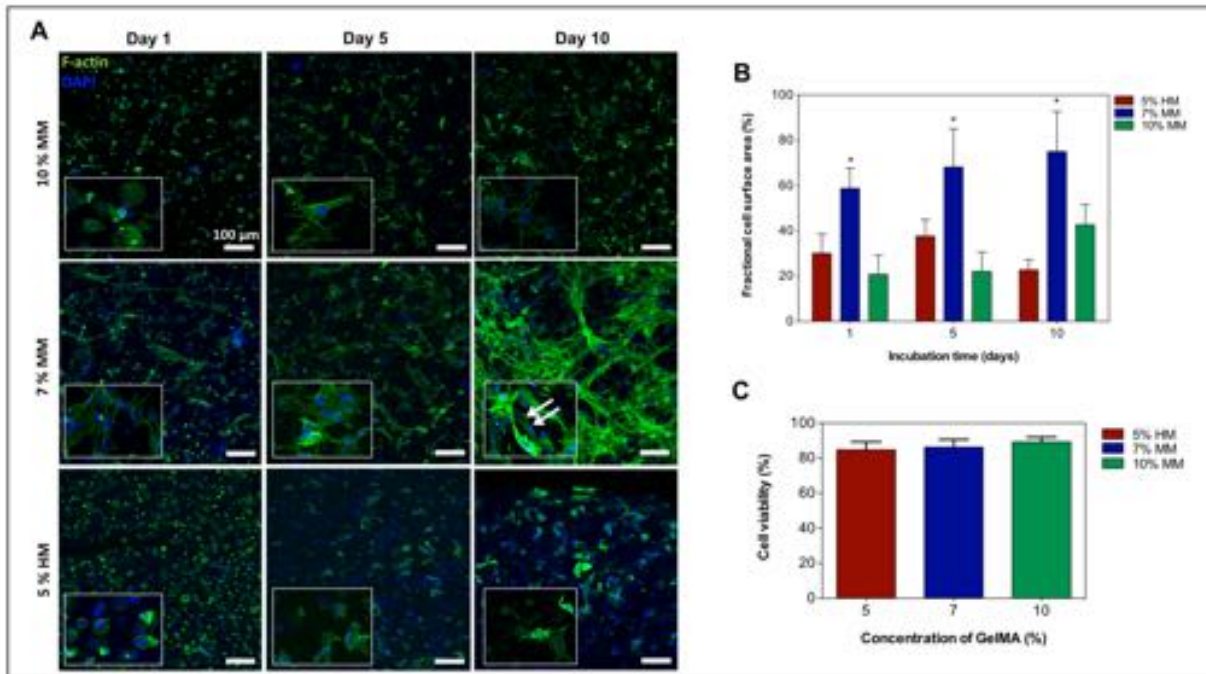
661

662



663

664 **Figure 2. Mechanical, porosity and degradation properties of GelMA hydrogels.** A) pre  
665 modulus of GelMA-hydrogels varies with different macromer concentration and degree of  
666 methacryloyl modification. B) Pore size analysis of GelMA hydrogels. C) Degradation of  
667 GelMA hydrogels with various macromer concentration and methacryloyl modification degree in  
668 the presence of collagenase. D) Cross-Sectional scanning electron microscopy images of 5%  
669 HM-GelMA, 7% MM-GelMA, and 10% MM-GelMA hydrogels reveal different porosity. Data  
670 depict Mean  $\pm$  Standard deviation. \* $p < 0.05$



671 **Figure 3. Viability and spreading characteristics of cardiac fibroblasts and cardiomyocytes**  
 672 **encapsulated in mechanically tuned GelMA hydrogels.** A) Representative fluorescence  
 673 images of encapsulated cardiac fibroblasts and cardiomyocytes within various GelMA hydrogels  
 674 at day 1, 5, and 10 of culture. B) Representation of a quantitative analysis of fractional F-actin  
 675 coverage within selected windows of 400  $\mu\text{m}$  x 400  $\mu\text{m}$ . C) Quantitative analysis of the viability  
 676 of cardiomyocytes and cardiac fibroblasts within various GelMA hydrogels conditions on day 1  
 677 of culture. Data depict Mean  $\pm$  Standard deviation. \* $p < 0.05$

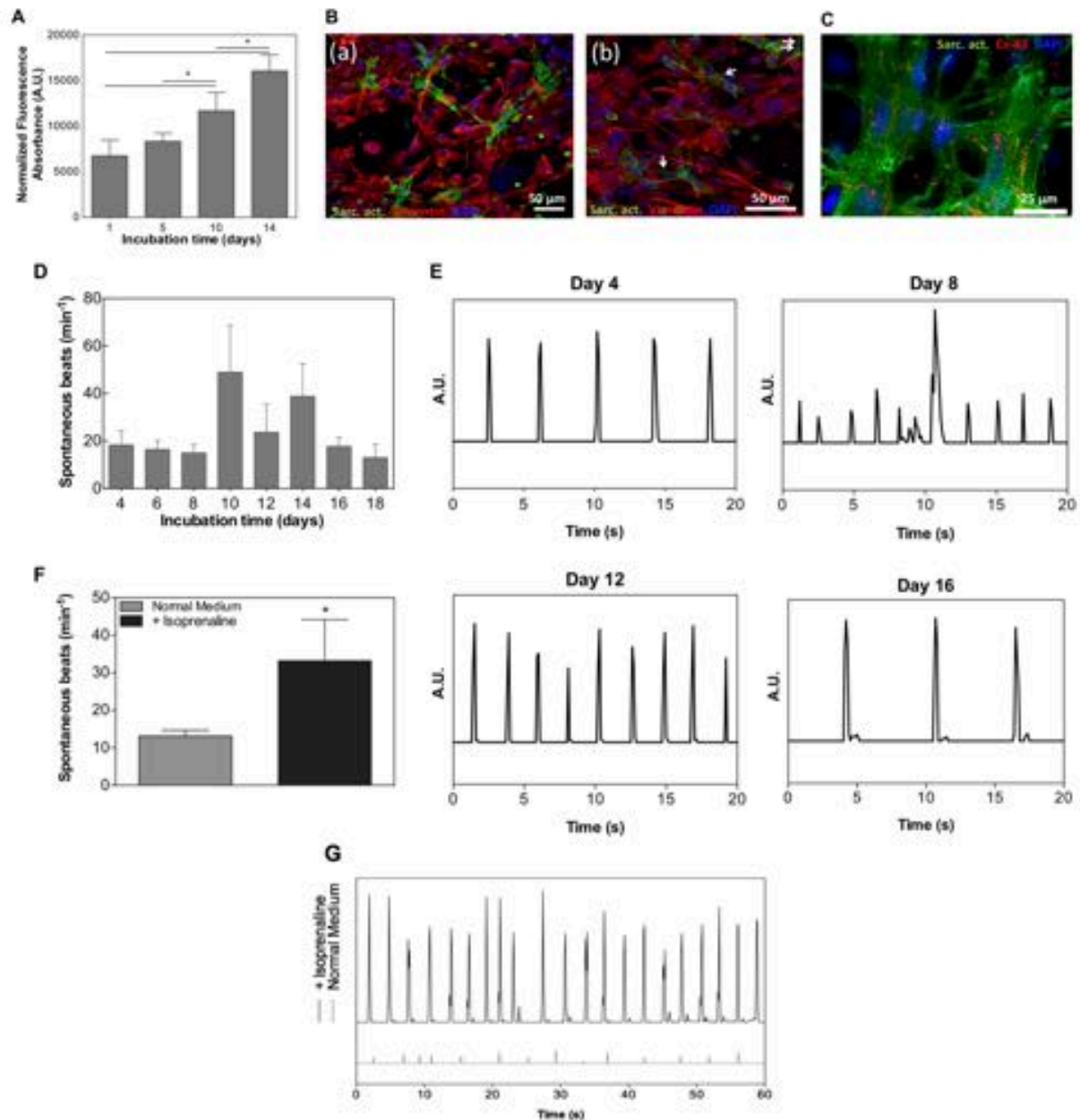
678

679

680

681

682



683

684

685

686

687

688

689

**Figure 4. Functional Properties of 3D engineered cardiac tissues.** **A)** Quantitative analysis of cellular metabolic activity throughout 14 days of culture. **B)** Representative fluorescence images of immunostained cardiomyocytes ( $\alpha$ -sarcomeric actin = green) and cardiac fibroblasts (vimentin = red) on day 14 of culture (a). Higher magnification images of immunostained cardiomyocytes and cardiac fibroblasts showed sarcomeric cross-striations (white arrows) (b). **C)** Fluorescent image showing well developed sarcomeric striations (= green) and the expression of a gap-

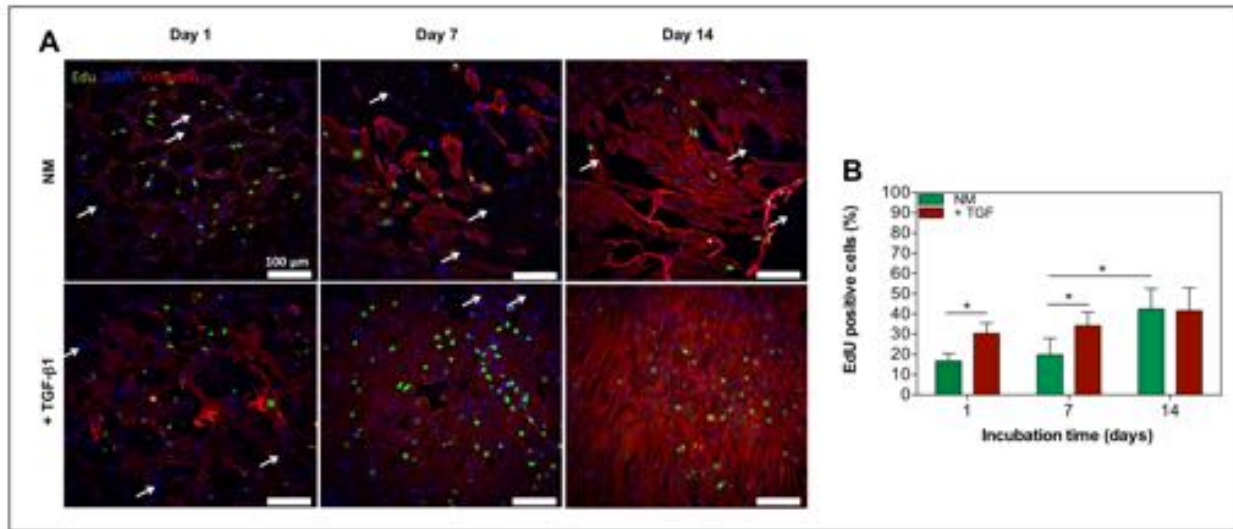
690 junctional protein, connexin-43 (= red). **D)** Quantitative representation of the spontaneous beats  
691 per minute of 3D engineered cardiac tissues from day 4 up until a maximum of 18 days of  
692 culture. **E)** Representative beating pattern of the cardiac tissues at day 4, 8, 12, and 16 of culture.  
693 **F)** Quantitative analysis of the spontaneous beats per minute of cardiac tissues (n=3) in the  
694 absence and presence of 1 $\mu$ M isoproterenol (isoprenaline). **G)** Representation of the beating  
695 pattern of cardiac tissues in the absence and presence of isoproterenol at day 6. Data depict Mean  
696  $\pm$  Standard deviation. \* $p$ <0.05

697

698

699

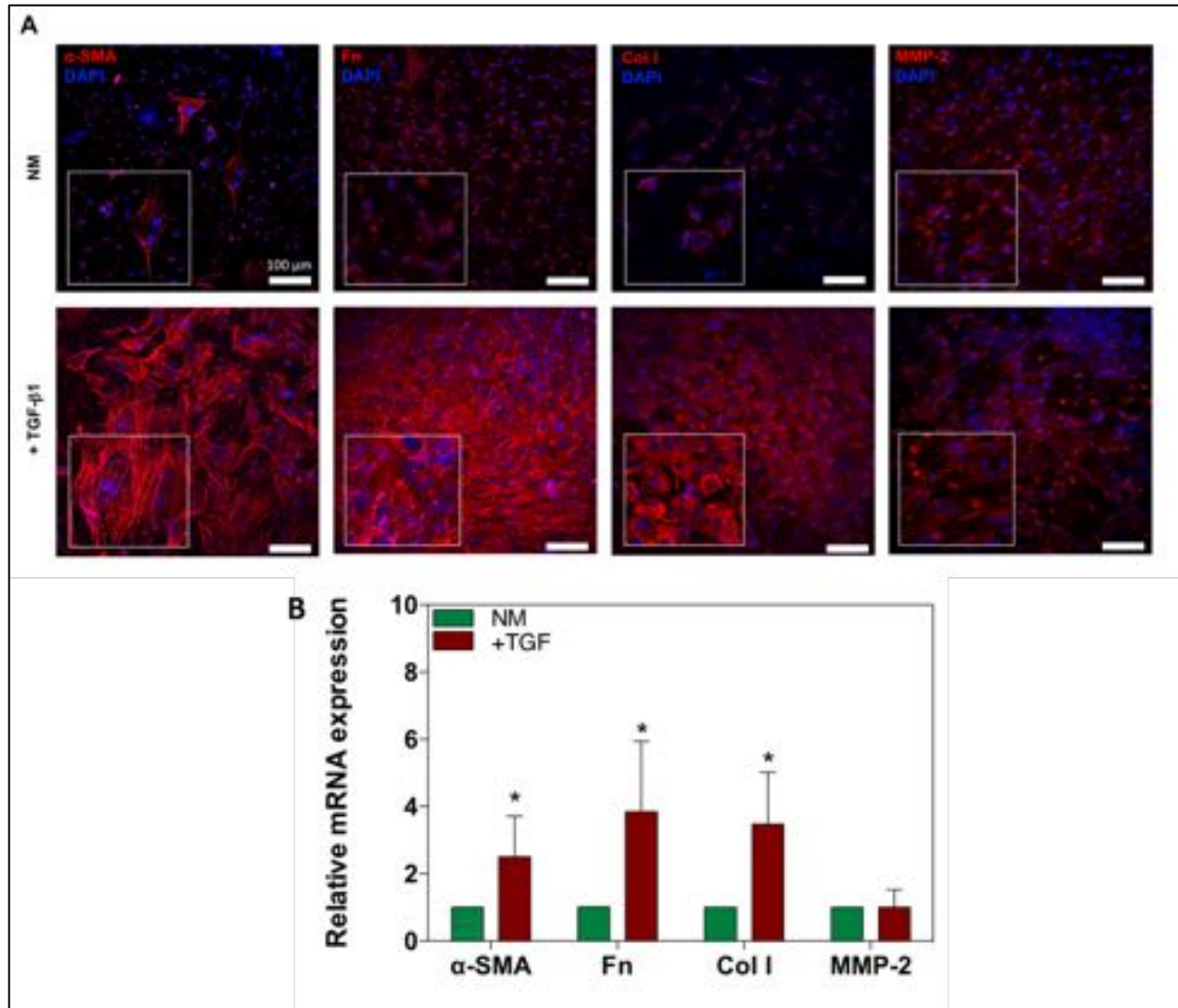
CONFIDENTIAL



700  
 701 **Figure 5. The exogenous addition of TGF-β1 affects proliferation of cardiac fibroblasts in**  
 702 **3D engineered cardiac tissues. A)** Confocal images of immunofluorescence staining of a  
 703 cardiac fibroblast marker, vimentin (= red), and EdU click-iT labeling (= green) of 3D  
 704 engineered cardiac tissues with and without the addition of TGF-β1 at day 1, 7, and 14.  
 705 Cardiomyocytes were not stained and showed no positive EdU labeling (white arrows) **B)**  
 706 Representative quantification of proliferating cells inside 3D cardiac tissues as determined by the  
 707 percentage of EdU positive cells at day 1, 7, and 14 of culture (n=3). Data depict Mean ±  
 708 Standard deviation. \* $p < 0.05$

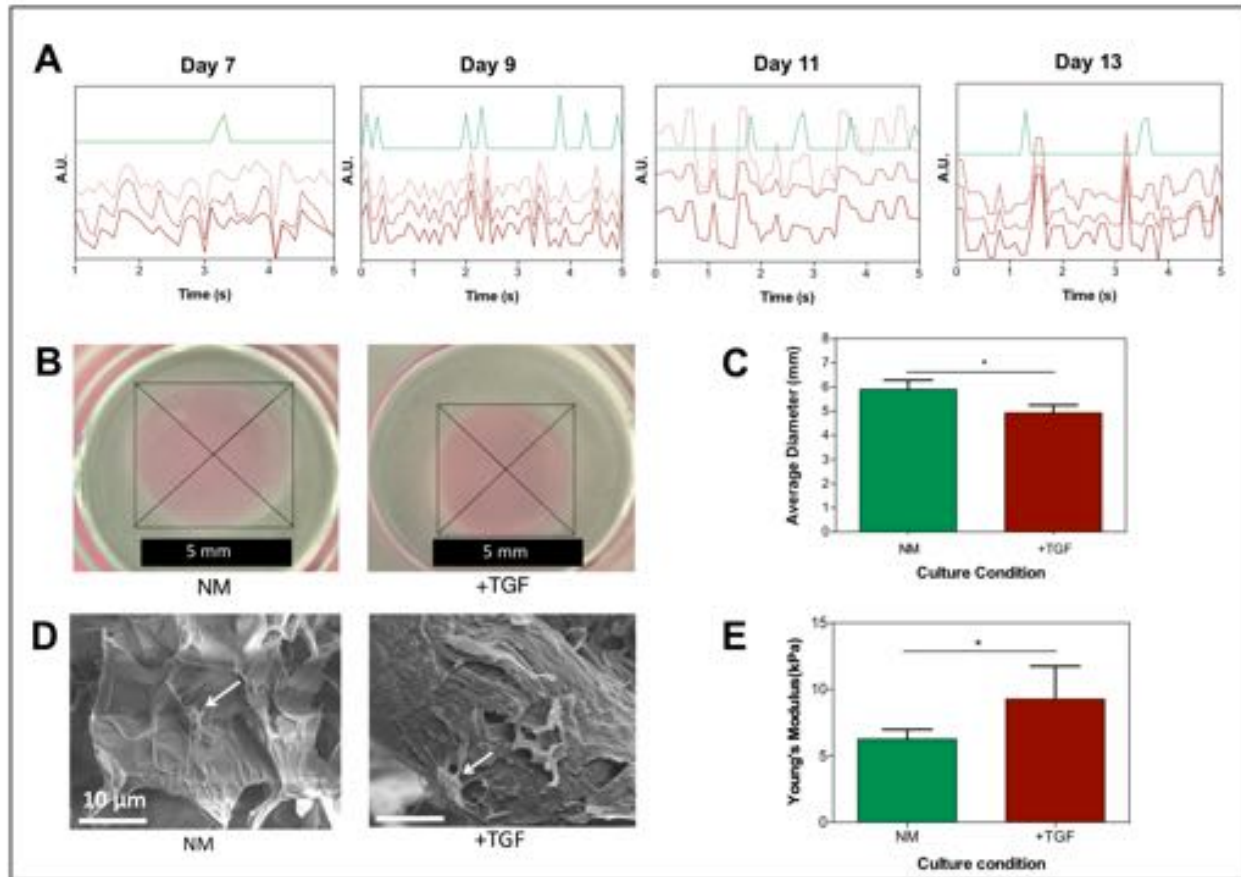
709

710



711

712 **Figure 6. Increased expression of fibrotic makers and increased differentiation of quiescent**  
 713 **cardiac fibroblasts into MyoFs by TGF- $\beta$ 1.** A) Confocal images of immunofluorescence  
 714 stained markers of cardiac fibrosis and MyoF differentiation;  $\alpha$ -SMA, collagen-I (Col I),  
 715 fibronectin (Fn), and MMP-2 after 14 days of culture. B) Data representing RT-PCR of mRNA  
 716 expression of  $\alpha$ -SMA, collagen-I, fibronectin, and MMP-2 in normal culture medium (NM)  
 717 compared to NM + TGF- $\beta$ 1 after 14 days of culture. Data depict fold-change  $\pm$  standard  
 718 deviation. \* $p < 0.05$ .



719

720 **Figure 7. TGF- $\beta$ 1 induces pro-fibrotic changes, such as increased contractility of hydrogels,**  
 721 **increased mechanical stiffness, and asynchronous beating, in 3D engineered cardiac tissues.**

722 **A)** Beating patterns of 3D engineered cardiac tissues cultured in NM (green) and NM + TGF- $\beta$ 1  
 723 (red) at day 7, 9, 11, and 13. The three red lines (solid and 3dotted) represent three independently  
 724 areas of beating within the same area of view. **B)** Hydrogel contraction test. Optical images of  
 725 TGF- $\beta$ 1 treated and non-treated hydrogels with encapsulated cardiomyocytes and cardiac  
 726 fibroblasts. **C)** Quantitative analysis of the contraction test of cardiomyocytes/cardiac fibroblast  
 727 encapsulated GelMA hydrogels in NM compared to NM + TGF- $\beta$ 1. **D)** Representative scanning  
 728 electron microscopy images of cell (white arrows)-encapsulated GelMA hydrogels cultured in  
 729 NM and NM + TGF- $\beta$ 1 on day 14 of culture. **E)** Mechanical stiffness of the 3D cardiac tissues in

730 the two different culture conditions (NM and NM+TGF-β1) at day 14 of culture. Data depict

731 Mean ± Standard deviation. \* $p < 0.05$

732

733

734

735

736

737

738

739

740

741

742

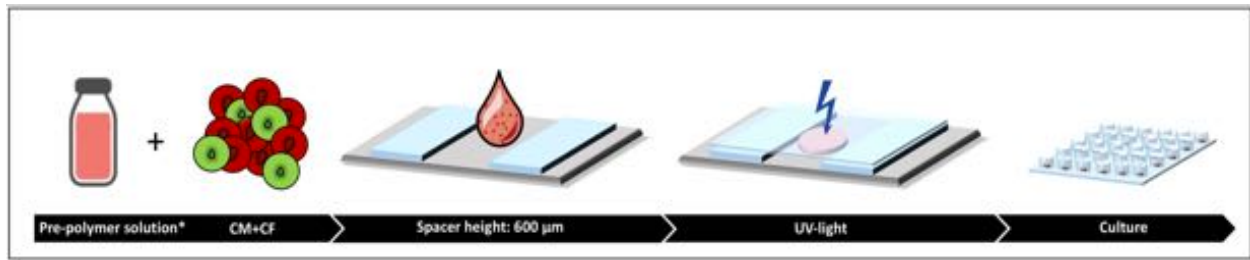
743

744

745

CONFIDENTIAL

746 **Supplemental information**



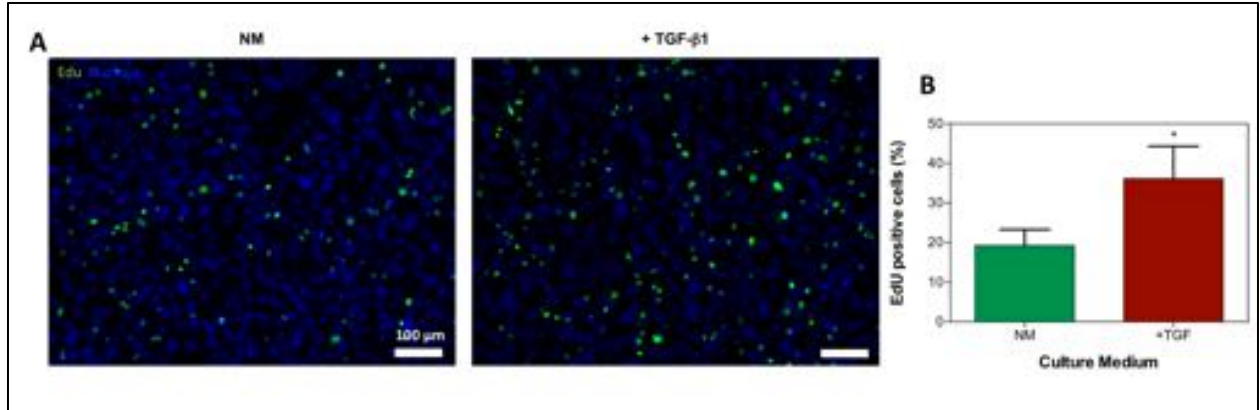
748 **Supplemental figure 1. Encapsulation of cardiomyocytes and cardiac fibroblasts within**  
749 **GelMA hydrogels.** Primary neonatal rat cardiomyocytes and cardiac fibroblasts are isolated and  
750 resuspended in a GelMA-based pre-polymer solution. Twelve microliters of the cell-laden pre-  
751 polymer solution is pipetted between two spacers with 600  $\mu\text{m}$  height. A sterile TMSPMA  
752 treated glass slide is placed on top of this cell-laden GelMA solution and subsequently cross-  
753 linked by UV-exposure for 20 s. This was followed by the separation of the hydrogels from the  
754 glass slide by a thin coverslip to culture the Cell-laden GelMA solution in a 48-well plate.

755

756

757

758



759

760 **Supplemental figure 2. EdU labeling of cardiac fibroblasts cultured on TCPS. A)**

761 Fluorescence images of positive EdU labeled cardiac fibroblasts with and without TGF-β1, after

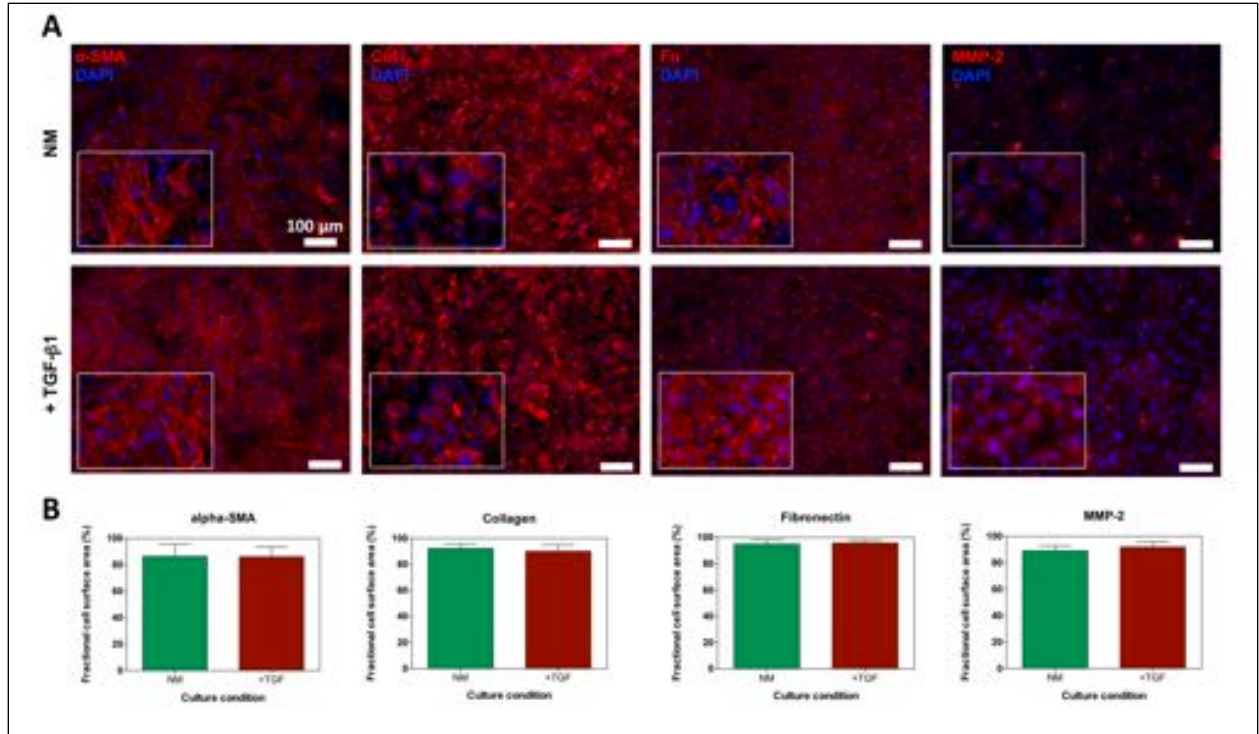
762 24h of culture. **B)** Representative quantification of proliferating cardiac fibroblasts in both the

763 presence (+TGF-β1) and absence (NM) of TGF-β1 after 24h of culture. Data depict Mean ±

764 Standard deviation. \* $p < 0.05$

765

766



767

768 **Supplemental figure 3. Expression profiles of cardiac fibrosis markers in cardiac**  
 769 **fibroblasts cultured on TCPS. A).** Fluorescence images of cardiac fibrosis markers; alpha-  
 770 smooth muscle actin ( $\alpha$ -SMA), collagen-I (col I), fibronectin (Fn), and matrix metalloproteinase-  
 771 2 (MMP-2) in the presence and absence of TGF- $\beta$ 1, after 24h of culture. **B)** Representation of a  
 772 quantitative analysis of fractional cell surface area. Data depict Mean  $\pm$  Standard deviation.

773

774

775

776

777

778 **References**

- 779 1 WHO. Cardiovascular <http://www.who.int/mediacentre/factsheets/fs317/en/>  
780 (2015).
- 781 2 Mozaffarian, D. *et al.* Heart disease and stroke statistics--2015 update: a report from the  
782 American Heart Association. *Circulation* **131**, e29-322,  
783 doi:10.1161/CIR.000000000000152 (2015).
- 784 3 Sutton, M. G. & Sharpe, N. Left ventricular remodeling after myocardial infarction:  
785 pathophysiology and therapy. *Circulation* **101**, 2981-2988 (2000).
- 786 4 Deddens, J. C. *et al.* Modeling the Human Scarred Heart In Vitro: Toward New Tissue  
787 Engineered Models. *Adv. Healthcare Mater.* **0**, 1-20 (2016).
- 788 5 Heusch, G. *et al.* Cardiovascular remodelling in coronary artery disease and heart failure.  
789 *Lancet* **383**, 1933-1943, doi:10.1016/S0140-6736(14)60107-0 (2014).
- 790 6 Weber, K. T., Sun, Y., Bhattacharya, S. K., Ahokas, R. A. & Gerling, I. C.  
791 Myofibroblast-mediated mechanisms of pathological remodelling of the heart. *Nat Rev*  
792 *Cardiol* **10**, 15-26, doi:10.1038/nrcardio.2012.158 (2013).
- 793 7 Hermans, K. C., Daskalopoulos, E. P. & Blankesteyjn, W. M. The Janus face of  
794 myofibroblasts in the remodeling heart. *J Mol Cell Cardiol* **91**, 35-41,  
795 doi:10.1016/j.yjmcc.2015.11.017 (2016).
- 796 8 Leask, A. Potential therapeutic targets for cardiac fibrosis: TGFbeta, angiotensin,  
797 endothelin, CCN2, and PDGF, partners in fibroblast activation. *Circ Res* **106**, 1675-1680,  
798 doi:10.1161/CIRCRESAHA.110.217737 (2010).
- 799 9 Kong, P., Christia, P. & Frangogiannis, N. G. The pathogenesis of cardiac fibrosis. *Cell*  
800 *Mol Life Sci* **71**, 549-574, doi:10.1007/s00018-013-1349-6 (2014).
- 801 10 Rockey, D. C., Bell, P. D. & Hill, J. A. Fibrosis--A Common Pathway to Organ Injury  
802 and Failure. *N Engl J Med* **373**, 96, doi:10.1056/NEJMc1504848 (2015).
- 803 11 Deb, A. & Ubil, E. Cardiac fibroblast in development and wound healing. *J Mol Cell*  
804 *Cardiol* **70**, 47-55, doi:10.1016/j.yjmcc.2014.02.017 (2014).
- 805 12 Creemers, E. E., Cleutjens, J. P., Smits, J. F. & Daemen, M. J. Matrix metalloproteinase  
806 inhibition after myocardial infarction: a new approach to prevent heart failure? *Circ Res*  
807 **89**, 201-210 (2001).
- 808 13 Rohr, S. Myofibroblasts in diseased hearts: new players in cardiac arrhythmias? *Heart*  
809 *Rhythm* **6**, 848-856, doi:10.1016/j.hrthm.2009.02.038 (2009).
- 810 14 Hill, J. A. & Olson, E. N. Cardiac plasticity. *N Engl J Med* **358**, 1370-1380,  
811 doi:10.1056/NEJMra072139 (2008).
- 812 15 Bujak, M. & Frangogiannis, N. G. The role of TGF-beta signaling in myocardial  
813 infarction and cardiac remodeling. *Cardiovasc Res* **74**, 184-195,  
814 doi:10.1016/j.cardiores.2006.10.002 (2007).
- 815 16 Schroer, A. K. & Merryman, W. D. Mechanobiology of myofibroblast adhesion in  
816 fibrotic cardiac disease. *J Cell Sci* **128**, 1865-1875, doi:10.1242/jcs.162891 (2015).
- 817 17 Yong, K. W. *et al.* Mechanoregulation of cardiac myofibroblast differentiation:  
818 implications for cardiac fibrosis and therapy. *Am J Physiol Heart Circ Physiol* **309**,  
819 H532-542, doi:10.1152/ajpheart.00299.2015 (2015).
- 820 18 Brown, R. D., Ambler, S. K., Mitchell, M. D. & Long, C. S. The cardiac fibroblast:  
821 therapeutic target in myocardial remodeling and failure. *Annu Rev Pharmacol Toxicol* **45**,  
822 657-687, doi:10.1146/annurev.pharmtox.45.120403.095802 (2005).

- 823 19 Benam, K. H. *et al.* Engineered in vitro disease models. *Annu Rev Pathol* **10**, 195-262,  
824 doi:10.1146/annurev-pathol-012414-040418 (2015).
- 825 20 Saini, H., Navaei, A., Van Putten, A. & Nikkhah, M. 3D cardiac microtissues  
826 encapsulated with the co-culture of cardiomyocytes and cardiac fibroblasts. *Adv Healthc*  
827 *Mater* **4**, 1961-1971, doi:10.1002/adhm.201500331 (2015).
- 828 21 Zimmermann, W. H. *et al.* Tissue engineering of a differentiated cardiac muscle  
829 construct. *Circ Res* **90**, 223-230 (2002).
- 830 22 Hirt, M. N. *et al.* Increased afterload induces pathological cardiac hypertrophy: a new in  
831 vitro model. *Basic Res Cardiol* **107**, 307, doi:10.1007/s00395-012-0307-z (2012).
- 832 23 Nichol, J. W. *et al.* Cell-laden microengineered gelatin methacrylate hydrogels.  
833 *Biomaterials* **31**, 5536-5544, doi:S0142-9612(10)00448-5 [pii]  
10.1016/j.biomaterials.2010.03.064 (2010).
- 834 24 Zhao, H. *et al.* Microengineered in vitro model of cardiac fibrosis through modulating  
835 myofibroblast mechanotransduction. *Biofabrication* **6**, 045009, doi:10.1088/1758-  
836 5082/6/4/045009 (2014).
- 837 25 Hjortnaes, J. *et al.* Directing valvular interstitial cell myofibroblast-like differentiation in  
838 a hybrid hydrogel platform. *Adv Healthc Mater* **4**, 121-130,  
839 doi:10.1002/adhm.201400029 (2015).
- 840 26 Galie, P. A., Westfall, M. V. & Stegemann, J. P. Reduced serum content and increased  
841 matrix stiffness promote the cardiac myofibroblast transition in 3D collagen matrices.  
842 *Cardiovasc Pathol* **20**, 325-333, doi:10.1016/j.carpath.2010.10.001 (2011).
- 843 27 Khademhosseini, A. *et al.* Microfluidic patterning for fabrication of contractile cardiac  
844 organoids. *Biomed Microdevices* **9**, 149-157, doi:10.1007/s10544-006-9013-7 (2007).
- 845 28 Kim, S. B. *et al.* A cell-based biosensor for real-time detection of cardiotoxicity using  
846 lensfree imaging. *Lab Chip* **11**, 1801-1807, doi:10.1039/c1lc20098d (2011).
- 847 29 Bhana, B. *et al.* Influence of substrate stiffness on the phenotype of heart cells.  
848 *Biotechnol Bioeng* **105**, 1148-1160, doi:10.1002/bit.22647 (2010).
- 849 30 Vlierberghe, S. V. *et al.* Porous gelatin hydrogels: 1. Cryogenic formation and structure  
850 analysis. *Biomacromolecules* **8**, 331-337, doi:10.1021/bm060684o (2007).
- 851 31 Spinale, F. G. Matrix metalloproteinases: regulation and dysregulation in the failing  
852 heart. *Circ Res* **90**, 520-530 (2002).
- 853 32 Kreuzberg, M. M., Willecke, K. & Bukauskas, F. F. Connexin-mediated cardiac impulse  
854 propagation: connexin 30.2 slows atrioventricular conduction in mouse heart. *Trends*  
855 *Cardiovasc Med* **16**, 266-272, doi:10.1016/j.tcm.2006.05.002 (2006).
- 856 33 Shin, S. R. *et al.* Carbon-nanotube-embedded hydrogel sheets for engineering cardiac  
857 constructs and bioactuators. *ACS Nano* **7**, 2369-2380, doi:10.1021/nn305559j (2013).
- 858 34 Annabi, N. *et al.* Highly Elastic Micropatterned Hydrogel for Engineering Functional  
859 Cardiac Tissue. *Adv Funct Mater* **23**, doi:10.1002/adfm.201300570 (2013).
- 860 35 Radisic, M. *et al.* Medium perfusion enables engineering of compact and contractile  
861 cardiac tissue. *Am J Physiol Heart Circ Physiol* **286**, H507-516,  
862 doi:10.1152/ajpheart.00171.2003 (2004).
- 863 36 Hinz, B. The myofibroblast: paradigm for a mechanically active cell. *J Biomech* **43**, 146-  
864 155, doi:10.1016/j.jbiomech.2009.09.020 (2010).
- 865 37 Thompson, S. A., Copeland, C. R., Reich, D. H. & Tung, L. Mechanical coupling  
866 between myofibroblasts and cardiomyocytes slows electric conduction in fibrotic cell  
867

868 monolayers. *Circulation* **123**, 2083-2093, doi:10.1161/CIRCULATIONAHA.110.015057  
869 (2011).

870 38 Janmey, P. A. & Miller, R. T. Mechanisms of mechanical signaling in development and  
871 disease. *J Cell Sci* **124**, 9-18, doi:10.1242/jcs.071001 (2011).

872 39 Engler, A. J. *et al.* Embryonic cardiomyocytes beat best on a matrix with heart-like  
873 elasticity: scar-like rigidity inhibits beating. *J Cell Sci* **121**, 3794-3802,  
874 doi:10.1242/jcs.029678 (2008).

875 40 Ma, Y., Halade, G. V. & Lindsey, M. L. Extracellular matrix and fibroblast  
876 communication following myocardial infarction. *J Cardiovasc Transl Res* **5**, 848-857,  
877 doi:10.1007/s12265-012-9398-z (2012).

878 41 Stawowy, P. *et al.* Regulation of matrix metalloproteinase MT1-MMP/MMP-2 in cardiac  
879 fibroblasts by TGF-beta1 involves furin-convertase. *Cardiovasc Res* **63**, 87-97,  
880 doi:10.1016/j.cardiores.2004.03.010 (2004).

881 42 Shamhart, P. E. & Meszaros, J. G. Non-fibrillar collagens: key mediators of post-  
882 infarction cardiac remodeling? *J Mol Cell Cardiol* **48**, 530-537,  
883 doi:10.1016/j.yjmcc.2009.06.017 (2010).

884 43 van den Borne, S. W. *et al.* Myocardial remodeling after infarction: the role of  
885 myofibroblasts. *Nat Rev Cardiol* **7**, 30-37, doi:10.1038/nrcardio.2009.199 (2010).

886 44 Rosenkranz, S. TGF-beta1 and angiotensin networking in cardiac remodeling.  
887 *Cardiovasc Res* **63**, 423-432, doi:10.1016/j.cardiores.2004.04.030 (2004).

888 45 Tomasek, J. J., Gabbiani, G., Hinz, B., Chaponnier, C. & Brown, R. A. Myofibroblasts  
889 and mechano-regulation of connective tissue remodelling. *Nat Rev Mol Cell Biol* **3**, 349-  
890 363, doi:10.1038/nrm809 (2002).

891 46 Bergmann, O. *et al.* Evidence for cardiomyocyte renewal in humans. *Science* **324**, 98-  
892 102, doi:10.1126/science.1164680 (2009).

893 47 Chen, M. B., Srigunapalan, S., Wheeler, A. R. & Simmons, C. A. A 3D microfluidic  
894 platform incorporating methacrylated gelatin hydrogels to study physiological  
895 cardiovascular cell-cell interactions. *Lab Chip* **13**, 2591-2598, doi:10.1039/c3lc00051f  
896 (2013).

897 48 Discher, D. E., Janmey, P. & Wang, Y. L. Tissue cells feel and respond to the stiffness of  
898 their substrate. *Science* **310**, 1139-1143, doi:10.1126/science.1116995 (2005).

899 49 Yue, K. *et al.* Synthesis, properties, and biomedical applications of gelatin methacryloyl  
900 (GelMA) hydrogels. *Biomaterials* **73**, 254-271, doi:10.1016/j.biomaterials.2015.08.045  
901 (2015).

902 50 Ott, H. C. *et al.* Perfusion-decellularized matrix: using nature's platform to engineer a  
903 bioartificial heart. *Nat Med* **14**, 213-221, doi:10.1038/nm1684 (2008).

904 51 Williams, C. *et al.* Cardiac extracellular matrix-fibrin hybrid scaffolds with tunable  
905 properties for cardiovascular tissue engineering. *Acta Biomater* **14**, 84-95,  
906 doi:10.1016/j.actbio.2014.11.035 (2015).

907 52 Visser, J. *et al.* Crosslinkable hydrogels derived from cartilage, meniscus, and tendon  
908 tissue. *Tissue Eng Part A* **21**, 1195-1206, doi:10.1089/ten.TEA.2014.0362 (2015).

909 53 Ingber, D. E. Cellular mechanotransduction: putting all the pieces together again. *FASEB*  
910 *J* **20**, 811-827, doi:10.1096/fj.05-5424rev (2006).

911 54 Bokel, C. & Brown, N. H. Integrins in development: moving on, responding to, and  
912 sticking to the extracellular matrix. *Dev Cell* **3**, 311-321 (2002).

- 913 55 Israeli-Rosenberg, S., Manso, A. M., Okada, H. & Ross, R. S. Integrins and integrin-  
914 associated proteins in the cardiac myocyte. *Circ Res* **114**, 572-586,  
915 doi:10.1161/CIRCRESAHA.114.301275 (2014).
- 916 56 Leckband, D. E., le Duc, Q., Wang, N. & de Rooij, J. Mechanotransduction at cadherin-  
917 mediated adhesions. *Curr Opin Cell Biol* **23**, 523-530, doi:10.1016/j.ceb.2011.08.003  
918 (2011).
- 919 57 Chiquet, M., Gelman, L., Lutz, R. & Maier, S. From mechanotransduction to  
920 extracellular matrix gene expression in fibroblasts. *Biochim Biophys Acta* **1793**, 911-920,  
921 doi:10.1016/j.bbamcr.2009.01.012 (2009).
- 922 58 Sheehy, S. P., Grosberg, A. & Parker, K. K. The contribution of cellular  
923 mechanotransduction to cardiomyocyte form and function. *Biomech Model Mechanobiol*  
924 **11**, 1227-1239, doi:10.1007/s10237-012-0419-2 (2012).
- 925 59 Kim, D. H. *et al.* Nanoscale cues regulate the structure and function of macroscopic  
926 cardiac tissue constructs. *Proc Natl Acad Sci U S A* **107**, 565-570,  
927 doi:10.1073/pnas.0906504107 (2010).
- 928 60 Pijnappels, D. A., Gregoire, S. & Wu, S. M. The integrative aspects of cardiac  
929 physiology and their implications for cell-based therapy. *Ann N Y Acad Sci* **1188**, 7-14,  
930 doi:10.1111/j.1749-6632.2009.05077.x (2010).
- 931 61 Papadaki, M. *et al.* Tissue engineering of functional cardiac muscle: molecular,  
932 structural, and electrophysiological studies. *Am J Physiol Heart Circ Physiol* **280**, H168-  
933 178 (2001).
- 934 62 Au, H. T., Cheng, I., Chowdhury, M. F. & Radisic, M. Interactive effects of surface  
935 topography and pulsatile electrical field stimulation on orientation and elongation of  
936 fibroblasts and cardiomyocytes. *Biomaterials* **28**, 4277-4293,  
937 doi:10.1016/j.biomaterials.2007.06.001 (2007).
- 938 63 Aubin, H. *et al.* Directed 3D cell alignment and elongation in microengineered hydrogels.  
939 *Biomaterials* **31**, 6941-6951, doi:10.1016/j.biomaterials.2010.05.056 (2010).
- 940 64 Bhatia, S. N. & Ingber, D. E. Microfluidic organs-on-chips. *Nat Biotechnol* **32**, 760-772,  
941 doi:10.1038/nbt.2989 (2014).
- 942 65 Ribas, J. *et al.* Cardiovascular Organ-on-a-Chip Platforms for Drug Discovery and  
943 Development  
944 *Applied In Vitro Toxicology* **2**, 82-96 (Jun 2016).
- 945
- 946
- 947